Precipitation variability within an urban monitoring network via microcanonical cascade generators

Paweł Licznar[1,*], Carlo De Michele[2], Witlod Adamowski[3]

[1] Institute of Environment Protection Engineering, Wrocław University of Technology, Wrocław, Poland.

[2] Department of Civil and Environmental Engineering, Politecnico di Milano, Italy.

[3] Institute of Environmental Engineering, John Paul II Catholic University of Lublin, Stalowa Wola, 37-450 Poland.

*Corresponding author; email: pawel.licznar@pwr.wroc.pl

Abstract

Understanding the variability of precipitation at small scales is fundamental in urban hydrology. Here we consider as case study Warsaw, Poland, characterized by a precipitation-monitoring network of 25 gauges, and as instrument of investigation the microcanonical cascades.

We address the following issues partially investigated in literature: 1) the calibration of microcanonical cascade generators in conditions of short time series (say, 2.5-5 yrs.); 2) the identification of the probability distribution of breakdown coefficients through ranking criteria; 3) the variability among the gauges of the monitoring network of the empirical distribution of breakdown coefficients.

In particular, 1) we introduce an overlapping moving window algorithm to determine the histogram of breakdown coefficients, and compare it with the classic non-overlapping moving window algorithm; 2) we compare the 2N-B distribution, which is a mixed distribution composed by two Normal (N) and one Beta (B), with the classic Beta distribution to represent the breakdown coefficients using the Akaike information criterion; 3) we use the cluster analysis to identify patterns of breakdown coefficient histograms among gauges and timescales.

The scarce representation of the breakdown coefficients at large timescales, due to the short period of observation (~2.5 yrs.), is solved through the overlapping moving window algorithm. BDC histograms are described by a 2N-B distribution. A clear evolution of this distribution is observed, in all gauges, from 2N-B at small timescales, to N-B at intermediate timescales, and to Beta distribution for large timescales.

The performance of the microcanonical cascades is evaluated for the considered gauges. Synthetic time series are analyzed with respect to the intermittency and the variability

of intensity, and compared to observed series. BDC histograms, for each timescale, are compared among the 25 gauges in Warsaw, and with other gauges located in Poland and Germany.

Key words: urban hydrology, precipitation time series, intermittency, microcanonical cascade, overlapping window, randomization, cluster analysis.

1 Introduction

Urban hydrology demands the access to very precise information about the precipitation variability over small spatial and temporal scales. Widespread use of surface runoff models coupled to urban drainage networks increases the common request for rainfall data inputs at high temporal and spatial resolutions. As it was already estimated a decade ago by Berne et al. (2004), the necessary resolution of rainfall data, as input of hydrological models, in Mediterranean regions, was about 5 min in time, and 3 km in space for urban catchments of ~1000 ha. For smaller urban catchments of ~100 ha, even higher resolutions of 3 min and 2 km were required. Results obtained with the application of operational semi-distributed urban hydrology models fully confirmed earlier observations on selected study cases from England and France (Gires et al. 2012, 2013). These authors strongly recommend the use of radar data in urban hydrology especially in context of real time control of urban drainage systems. In particular, they opted for X-band radars (whose resolution is hectometric), respect to the more common C-band radars, as affected by less uncertainty. Additionally, Gires et al. (2012) stated that small scale rainfall variability, under 1 km resolution, cannot be neglected, and should be accounted in probabilistic way in the real time management of urban drainage systems. As a matter of fact, the implementation of radar

techniques gained a rising popularity in major cities across the EU (for details refer to Appendix B, Thames Tunnel Needs Report, 2010).

Despite the obvious benefits of radar instruments, radar data are not always available for practical applications. Thus, current versions of even most advanced computer rainfall-runoff urban drainage models do not consider radar data as rainfall input. Therefore the only possibility of accounting spatial rainfall variability is to consider different point time series for each sub-catchment (Gires et al. 2012). The vast majority of engineering practical calculations and modeling of drainage systems is still associated with point rainfall time series, or their elaborations like intensity-duration-frequency (IDF) curves, or depth-duration-frequency (DDF) relations, or simplified design hyetographs. This explains the necessity of high temporal resolution of point rainfall measurements in urban catchments. It also has to be noticed that time series at high temporal resolution (1-10 minutes) and with a considerable record length (at least 20-30 years) are nowadays required especially from European perspective with respect to the probabilistic assessment of the urban drainage network functioning (Schmitt, 2000; European standard EN 752), or the probabilistic assessment of retention volumes at hydraulic overloaded stormwater systems (Arbeitsblatt DWA-A 117).

The strategy of using local precipitation time series as basis of the probabilistic assessment of urban drainage systems has two important shortcomings. In case of local precipitation data shortage, this strategy fails completely. Whereas, in all other situations, when some local precipitation datasets are accessible, questions and doubts about the representativeness and reliability of data arise. First of all, the doubts regard the temporal representativeness of data: short datasets could not allow to describe (as showed by Willems 2013) the multidecadal oscillatory behavior of rainfall extremes in stormwater outflow modeling. Other doubts regard the spatial representativeness of data: rainfall time series are recorded only in a limited number of gauges installed in selected sub-catchments. This results

in assigning the same time series to a group of neighboring sub-catchments, or in critical but not rare cases, one time series for the whole urban drainage system, habitually collected by a gauge installed nearby the airport. Sometimes, in situation of local precipitation shortage, time series from other locations are allowed by technical guidelines (Schmitt, 2000) only if there is compatibility in terms of annual precipitation totals, and IDF values.

Finally, since most of the modeling activity is oriented to predict the future behavior (e.g. in the next 50 yrs.) of drainage systems, the mere use of historical precipitation time series of the last 20-30 years could not be significant to represent the future scenarios. Alternatively, the generation of synthetic time series, from precipitation models, could represent probable precipitation scenarios to feed hydrodynamic urban drainage models and take into account the uncertainty associated to the discharge.

Thus, there is a strong motivation for the development of local precipitation models at high temporal resolutions. Many of them are based on the idea of precipitation disaggregation in time. The disaggregation refers to a technique generating consistent rainfall time series at some desired fine time scale (e.g. 5 min resolution) starting from the precipitation at a coarser scale (e.g. daily resolution). At the same time, as it was stressed by Lombardo et al. (2012), the downscaling techniques aim at producing fine-scale rain time series with statistics consistent with those of observed data. A general overview of rainfall disaggregation methods is given by Koutsoyiannis (2003). Among an ensemble of known techniques, random cascade models, and especially microcanonical cascade models (MCMs) are quite often used. The popularity of the latter ones could be explained by their appealing towards engineering applications, the assumption of mass conservation (i.e. rainfall depth conservation) across cascade levels, and straight rules for the extraction of cascade generators from local precipitation time series (Cârsteanu and Foufoula-Georgiou 1996). Olsson (1998), Menabde and Sivapalan (2000), Ahrens (2003), Paulson and Baxter (2007) provide contributions

110 demonstrating the potentiality of MCMs in rainfall downscaling. Molnar and Burlando (2005)
111 and Hingray and Ben Haha (2005) highlight the application of MCMs in urban hydrology.
112 Hingray and Ben Haha (2005) applied a continuous hydrological simulation obtaining from
113 synthetic rainfall series continuous discharge series used afterwards for the retention design.
114 Recently, Licznar (2013) illustrated the possibility of substituting synthetic time series
115 generated from MCMs to observed time series for the probabilistic design of stormwater
116 retention facilities.

117 Two decades of random cascade applications to precipitation disaggregation brought
118 progresses in the construction of generators. Quite soon, the assumption of independence and
119 identical distribution of the cascade weight generators, at all timescales, was questioned and
120 found suitable only for limited, rather narrow, range of analyzed scales (Olsson 1998, Harris
121 et al. 1998). As an alternative, Marshak et al. (1994), Menabde et al. (1997) and Harris et al.
122 (1998) promoted the use of the so-called "bounded" random cascade, for which its weights
123 distribution systematically evolves decreasing the weights variance with the reduction of
124 timescale. In addition, Rupp et al. (2009) suggested, that microcanonical cascade weights
125 should not be timescale-dependent only, but also intensity-dependent. The common practice
126 of assuming the Beta distribution for MCM generators was questioned by Licznar (2011a,b),
127 especially for sub-hourly timescales. Alternatively MCM generators were assumed Normal-
128 Beta (N-B) distributed with atom at 0.5, or 3N-B distributed, composed by three Normal and
129 one Beta distribution. For sake of clarity, it should be stressed that Beta refers sole to the
130 distribution of MCM generators, and has nothing in common with the beta β model, being the
131 simplest cascade model, often known as monofractal model (for details refer to Over and
132 Gupta 1996).

133 Molnar and Burlando (2008) explored the variability of MCM generators on a large
134 dataset of 10-min time resolution, including 62 stations across Switzerland. These authors

investigated seasonal and spatial variability in breakdown distributions to give indications concerning the parameters' estimation of MCM in ungauged locations. To our knowledge, this is the only study considering the large-scale variability of MCM generators, and there is a lack of knowledge concerning the small-scale variability.

It should be stressed that the fitting of cascade generators was relatively simple, but extremely data demanding. Observational precipitation time series of high resolution exceeding usually 20 years were unavoidable for cascade parameters fitting. This resulted in the prevailing practice of comparing the statistics of synthetic and observed time series. In the majority of studies, data originated from old type manual gauges were subject to obvious uncertainty related to the precision of measurements, as well as the resolution of records digitization. Simultaneously, the fitting of theoretical distributions to BDCs, in almost all cases, was not supported by statistical tests confirming the correctness of achieved results, or by the use of some information criteria to rank the theoretical distributions.

Having in mind the above discussed needs of urban hydrology, the current state of MCMs, and being fully aware of the severe limitations of this rainfall disaggregation technique, the goals of our study were:

1) Propose a methodology to calibrate microcanonical cascade generators in conditions of short time series;

2) Identify the probability distribution of BDCs through the use of information criterion;

3) Investigate the variability of empirical BDCs distributions among a group of gauges;

4) Address the following questions of interest in urban hydrology: "Is it acceptable to use a single time series for the probabilistic assessment of the entire urban drainage system? Is it sufficient to fit just one MCM for the analysis of the whole city area? Could we continue the practice of supplying urban rainfall-runoff models by time series recorded outside city center by gauges located at the airport or over rural areas?

2 Data and Methodology

2.1 Data

We use data belonging to a precipitation network of 25 gauges distributed throughout 517.24 km^2 of Warsaw city in Poland (Fig. 1). The dataset is the same used by Rupp et al. (2012) and consists in a 1-minute precipitation (both liquid and solid) time series recorded by electronic weighing-type gauges. All stations, TRwS 200E of MPS system Ltd. (Fig.2), were installed and operated by the Municipal Water Supply and Sewerage Company (MWSSC) in Warsaw. Prior to the network installation, studies about the location of the stations have been done by the MWSSC to identify the best configuration, representative of the precipitation variability within the urban area (Oke, 2006). All instruments were placed on grass, and their neighborhood met at least requirements of class 2 or 3, as recommended by WMO-No. 8. In the majority of gauges (i.e., R1, R3, R5, R7, R8, R10, R12, R17, R18 and R19) it was possible to install them on flat, horizontal surface, surrounded by an open area, meeting even requirements for class 1 instruments. In addition, gauge R15 was installed in perfect conditions on the ground at the Warsaw Fryderyk Chopin Airport.

Since the installation of the precipitation network in Warsaw was mainly motivated by the real time control of the drainage system, all gauges (Fig. 1) were connected to a single data acquisition system. The accuracy of gauge measurements, as claimed by manufacturer is 0.1%, and the data resolution is 0.001 mm for depth and 1 minute for time. As it was already mentioned by Rupp et al. (2012), field tests, conducted prior to the operational use of the precipitation network, have shown good agreement between simulated and recorded totals, and have revealed a dampening/broadening of the input signal, evident over the range of a few minutes. The last phenomenon, known as “step response error”, was studied in detail in laboratory conditions for different gauge types by Lanza et al. (2005). These found that the

step error of TRwS gauge is quite small in comparison to other gauges, and equal to 3 minutes in laboratory conditions. Our field test (as displayed on Fig. 2) suggested a dampening of gauge-recorded signal for the first 3-min initial phase of generated hyetograph and its slightly longer 5-min broadening at the final phase of hyetograph. Detailed discussion of the origins of gauge "step response" errors is beyond the scope of this manuscript, and in fact is hard to be realized, since it is introduced by gauge inner microprocessor algorithm of data processing. This algorithm is know-how of the gauge manufacturer, and is not reported in the technical documentation. In general, it could be only stated that in weighing type electronic gauges, the weight of deposed precipitation is sampled by some electronic (often piezometric) sensor with some high temporal resolution at presumably kHz rate. Afterwards all samples are averaged over longer time windows, unknown to the user. This process is repeated for overlapping time windows, and the difference of the rainfall total of adjacent windows is calculated to obtain the temporal rainfall rate reported as instrument output at its recording time resolution. In addition, rainfall rates are always rounded regardless of the magnitude of real precipitation (resulting in additional rounding errors discussed afterwards). This procedure allows for satisfying smoothing of electronic sensor signal fluctuation due to wind effects and temperature changes. It allows for the introduction of some additional filters cutting sudden signal jumps due to foreign objects deposition inside open orifice of the gauge inner tank (e.g. falling leaves or acts of vandalism by throwing small stones or garbage).

As a matter of fact in view of our personal experiences, and test results of WMO (Lanza et al. 2005), it could be stated that reliable precipitation recording at single minute scale by commercially available gauges is still the goal to be achieved, and not a current reality. Having this in mind, as well as timescales of previous microcanonical cascade studies concerning urban hydrology, realized on time series recorded by old-type gauges, we decided to work with the aggregated precipitation time series at 5-minute resolution. The technique

used to aggregate original 1-min data into 5-min time series is discussed afterwards; here we only mention that this operation was opposite to the rainfall total differentiation for adjacent time windows operated by the gauge microprocessor.

Despite the limited timespan of available data, covering the period from the 38th week of year 2008 up to the 49th week of year 2010, we believe that the Warsaw precipitation network might support good probing ground for the variability study in the microcanonical cascade parameters over small-scale urban areas. In fact, the Warsaw precipitation-monitoring network belongs to the biggest European urban gauge networks. Its size could be compared only with similar networks of 25 gauges in Vienna (414.87 km^2), or 24 gauges spread throughout Marseille (240.62 km^2) and Barcelona (100.4 km^2) (see Appendix B, Thames Tunnel Needs Report, 2010).

We compare the results of our study with those related to other Polish and German gauges. We limit our comparison to results previously published by Licznar et al. (2011a,b) for four gauges in Germany (gauges A, B, C and D - representing local climates of different parts of western Germany) and for one gauge in Wroclaw, Poland, and unpublished yet results by Górski (2013) for rain-gauge in Kielce, Poland (Fig. 3). Our choice is motivated by the similarity of the used methodology, and the investigated range of timescales, as well as by the indispensable accessibility to precise recordings of the breakdown coefficient histograms.

Finally, to investigate the existence of possible statistical bias induced by the calculation of BDCs on short precipitation records, we use additional data recorded by an old-type pluviograph gauge installed previously at the current location of gauge R7 on the ground of Lindley's Filters station. This pluviograph gauge was operated only in summer months from the May 1st to October 31st. Data were in the form of 15-min rainfall time series read off the original paper strips with the resolution of 0.1 mm for depth covering a period of 25-year from 1983 to 2007.

234 **2.2 Microcanonical cascade models**

235 We use microcanonical cascade models (MCMs) as in Licznar et al. (2011a,b). We
236 consider the disaggregation of precipitation totals from 1280-min (quasi daily) into 5-min
237 times series, assuming the branching number b equal to 2, and constructing cascades
238 assembled from only 9 levels (n=8, …, 1, 0) corresponding to timescales $\lambda=2^n$ from λ=256 to
239 λ=1 (Fig. 4). Precipitation depth time series generated by such cascades are the products of
240 the original precipitation total R_0 at timescale λ=256 multiplied by the sequence of weights at
241 the descending cascade levels:

242 $$R_{j,k} = R_0 \prod_{i=1}^{k} W_{f(i,j),i} \,, \tag{1}$$

243 where j=1, 2, …2^{k-1}, 2^k marks the position in the time series at the k^{th} cascade tier. The
244 sequence of randomly generated weights $W_{f(i,j),i}$ is steered at the following i^{th} cascade tier by
245 the function $f(i,j)$, which rounds up $j/2^{k-i}$ to the closest integer. The weights in the
246 microcanonical cascades are forced to sum to one, so their pairs are always equal to W and 1-
247 W respectively, where W is a two-sided truncated random variable from 0 to 1. The
248 microcanonical assumption conserves the mass (precipitation depth in our case) at each
249 branch, and eliminates the risk of cascade degeneration. From engineering perspective, this
250 means that the downscaling process could be seen as opposite to precipitation summation
251 realized by Hellman gauges, recording daily totals only, and a pragmatic solution for the
252 generation of synthetic precipitation time series at 5-minute resolution.

253 In our study we do not focus our attention on the disaggregation capabilities of
254 microcanonical cascades, already discussed in numerous papers. We concentrate on the small-
255 scale variability of their generators W among gauges constituting the urban precipitation
256 network. The obvious attractive of MCMs arises from the possibility of extracting the
257 distribution of W from data on the base of breakdown coefficients studies (Cârsteanu and

Foufoula-Georgiou 1996). By definition, BDCs are generally calculated using non-overlapping adjacent pairs of precipitation time series:

$$BDC_{j,\tau} = \frac{R_{j,\tau}}{R_{j,\tau} + R_{j+1,\tau}} \qquad j=1,3,5,\ldots,N_\tau\text{-}1; \qquad (2)$$

where $R_{j,\tau}$ is the precipitation amount for the time interval of length τ at position j in the time series, and N_τ is the length of time series at timescale τ. The calculation of BDCs with respect to Eq.(2) for Warsaw gauges is conducted only for nonzero pairs of R_j and R_{j+1}. Calculations are executed at aggregated intervals of length $2^n\tau_{org}$, where τ_{org} is the original time step equal to 5 min and n is a cascade level, increasing from 0 to 8, with increasing cascade timescales λ from 1 to 256 (Fig. 4). Simultaneously, for all analyzed timescales, BDC couples equal to 0 / 1, or 1 / 0 (when only one between R_j and R_{j+1} is zero) are separated from resulting datasets and their occurrence probabilities, respectively $p_0(LEFT)$ and $p_0(RIGHT)$ are used to estimate intermittency probability p_0:

$$\Pr(BDC_n(j) = 0 \; or \; BDC_n(j+1) = 0) = p_0(LEFT) + p_0(RIGHT) = p_0 . \qquad (3)$$

The probability p_0 is used within a MCM generator to take into account the intermittency, so characteristic of precipitation, forcing some portion of random weights W to be equal to 0.

The preliminary results have revealed an overrepresentation of BDC values equal to 1/2 or 1/3, 2/5, 1/4 (and 2/3, 3/5, 3/4 respectively), especially for small timescales, i.e. λ=1 and λ=2. Fig. 5 (left panel) shows an example of BDC histogram for timescale λ=1, with evident artificial spikes. Similar phenomenon was already reported by Rupp et al. (2009), and Licznar et al. (2011b), and explained as the result of instrument or recording precision of precipitation gauges. The magnitude of observed rounding errors for Warsaw gauges is however smaller than in case of German gauges (Licznar et al., 2011b), because the

precipitation depths were recorded with better resolution of 0.001 mm still however resulted in irregularity of BDCs distribution, induced by sharp peaks at discrete BDC values, and hindered the identification of the theoretical distribution. In order to correct the rounding errors, a randomization procedure originally proposed by Licznar et al. (2011b) was applied. This type of procedure, also known as jittering, is fundamental in the analysis of data characterized by the presence of ties, De Michele et al. (2013). Thus, the original 1-min time series were slightly modified by adding to the precipitation depths, exceeding zero, some random corrections. Random correction values were sampled from the Uniform distribution in the range [-0.0005, 0.0005] mm, resulting in visible BDCs histogram smoothing (Fig. 5 right panel). Note, that the Uniform distribution is used for the randomization of the rounding errors, because, in absence of information, it is the most intuitive distribution requiring less assumption, for more details please see Licznar et al. (2011b).

Irregularities in BDC histograms were observed for timescales $\lambda>8$. These are due to the decreasing sample size, calculated on limited timespan of accessible data, slightly exceeding 2 years. This issue was rather irrelevant in former studies (Molnar and Burlando 2005, 2008, Licznar et al. 2011a,b) realized on data series 10 or even 20 times longer. To solve this issue, we applied the overlapping moving window algorithm as an alternative to the classical non-overlapping moving window algorithm for the calculation of BDCs values. Figure 6 shows the differences between the two algorithms for $\lambda=1$. Switching from non-overlapping to overlapping moving window algorithm leads to increase the number of time segments for the calculation of BDCs values. For time series of n data, and a time window of size $m \leq n$, the number of non-overlapping windows is $\lfloor n/m \rfloor$, where the symbol $\lfloor \cdot \rfloor$ represents the integer part, while the number of overlapping windows is: $(n-m+1)$. For large $n>>m$, the overlapping moving window algorithm leads to almost m times the number of time segments

available in the overlapping moving window algorithm. It should be underlined that the real strength of the overlapping moving window algorithm in analyzing distributions of BDCs values could be observed for the largest timescales. The reason is that for small timescales, most of time segments is characterized by zero precipitation, and thus not involved in the calculation of BDCs, whereas for larger timescales, time segments are becoming larger and rarely characterized by zero precipitation. This phenomenon arises from the fractal properties of rainfall time series, and similar conclusions result from the "box-counting" analysis.

It is clear that the overlapping moving window algorithm is especially desired for limited observational datasets. However, its implementation for short time series may be characterized by a poor representativeness of BDCs distributions, due to multidecadal oscillations of precipitation totals and extremes (Willems 2013). To investigate the magnitude of the oscillations in the BDCs distributions, we use historical time series from former old-type gauge R7, covering a 25-year period, from 1983 to 2007 at 15-min resolution. For each year, there are available only 6 months of data from May to October. For this dataset, we make the calculations of BDCs in 7 time periods. First, we calculate BDCs for the following 5-year periods: 1983-1987, 1988-1992, 1993-1997, 1998-2002 and 2003-2007 using the overlapping moving window algorithm. We consider this temporal size (5 years × 6 months = 30 months) because comparable to the one available for electronic gauges. Afterwards, we repeat the same calculation with a 25-year long size using both non-overlapping and overlapping moving window algorithms. As we work here with a coarser resolution (15-min instead of 5-min of electronic gauges), we decide to perform the analysis with a smaller hierarchy of subdaily timescales λ' from 1 to 32 and breakdown times from 15-30 min up to 480-960 min. For all calculations we perform the randomization of nonzero values. Since their reading precision was set to 0.1 mm, we introduce a random correction belonging to the Uniform distribution in the range [-0.05, 0.05] mm.

To compare BDC histograms, obtained for all analyzed timescales λ and λ', with theoretical functions, a probability distribution assembling 2 truncated (with truncation points at 0 and 1) Normal distributions (Robert, 1995), and 1 Beta symmetrical distribution was implemented. This distribution, indicated as 2N-B distribution, has the following density function:

$$p(w) = p_1\left\{\frac{1}{\sigma_1\sqrt{2\pi}}e^{\frac{-(w-0.5)^2}{2\sigma_1^2}}\right\} + (1-p_1)\left\{p_2\left\{\frac{1}{B(a)}w^{a-1}(1-w)^{a-1}\right\} + (1-p_2)\left\{\frac{1}{\sigma_2\sqrt{2\pi}}e^{\frac{-(w-0.5)^2}{2\sigma_2^2}}\right\}\right\} \quad (4)$$

where p_1 and p_2 were weights characterizing the contribution of the individual distributions within the 2N-B distribution, σ_1 and σ_2 were the scale parameters of truncated Normal distributions, and $B(a)$ was the symmetrical Beta function, parameterized by a.

The fitting of 2N-B distribution parameters was performed numerically by means of maximum likelihood estimation. It is very likely, that the use of the model given in Eq.(4), governed by 5 parameters, could suffer of an over-parameterization, in comparison to the most commonly used Beta symmetrical distribution with only 1 parameter. Note that the application of goodness-of-fit tests (namely Kolmogorov-Smirnov test or χ^2 test) at 1% or 5% levels of significance gave negative result as for Beta as for 2N-B distribution. This because the large sample size of empirical BDCs has led to the rejection of the hypothesis, even in the case of very small differences between observed and theoretical distributions, as pointed out also in Licznar et al. (2011a). Here, we use the Akaike information criterion *AIC*, as a measure of the relative quality between 2N-B and Beta models for given sets of empirical BDCs. *AIC* is the maximized value of the log-likelihood function (*LL*) penalized by the number of model parameters *k*:

$$AIC=2k-2LL \quad (5)$$

The preferred distribution is the one with the minimum value of *AIC*.

352

353 **2.3 Cluster analysis**

354 To our knowledge, until now, the variability of MCM generators among a group of
355 gauges was investigated comparing the value of the parameter of Beta distribution (Molnar
356 and Burlando 2008). Here, we preferred to compare directly the empirical distribution of
357 BDCs instead of the parameters of the theoretical distribution, possibly biased by fitting
358 errors. We have encountered the same problems found in the implementation of statistical
359 tests due to the large sample size. For this, we have used the cluster analysis technique to
360 compare the shape of BDC histograms among the stations of the monitoring network in
361 Warsaw, and with other Polish and German gauges.

362 In particular a *hierarchical clustering* is used. This is a data-mining tool, applied to
363 segment data into relatively homogeneous subgroups, or clusters, where the similarity of the
364 records within the cluster is maximized (Larose, 2005). Prior the application of the clustering
365 technique, for each timescale and each site, the BDC histogram is sampled in 100 points,
366 selected at equal distance one from the following one. These 100 values are the components
367 of a vector representing the empirical BDC distribution. Note that a basic requirement of
368 cluster analysis is the comparison of records of equal length. As, all BDCs distributions are
369 left and right truncated, in the interval (0,1), sampling their histograms with a resolution of
370 0.01 produces vectors, which describe well the shape of histograms. The clustering of these
371 vectors (searching similar sites) is operated using the Euclidean distance. It is computed as:

372 $$d_{Euclidean}(X,Y) = \sqrt{\sum_i (x_i - y_i)^2}\,, \qquad (6)$$

373 where x_i and y_i with i=1,…,100, represent respectively the i-th component of X and Y vectors.

The Euclidean distance is a measure of similarity, not having, in general, a physical interpretation. Initially, in hierarchical clustering analysis, each vector is considered to be a tiny cluster of its own. Then, in following steps, the two closest clusters are aggregated into a new combined cluster. By replication of this operation, the number of clusters is reduced by one at each step and eventually, sites are combined into a single huge cluster. During the agglomerative process, the distance between clusters is determined based on single-linkage criterion. In this case, the distance between two clusters A and B is defined as the minimum distance between any element in cluster A and any element in cluster B. With respect to this single-linkage is often termed the nearest-neighbor approach, and tends to form long, slender clusters, clearly indicating similarities among clustered elements. As a final result of agglomerative clustering a treelike cluster structure (named dendrogram) is created.

Dendrograms show similarities, as well as dissimilarities, of BDC distributions among the considered sites and they are prepared separately for all analyzed timescales. In addition, the cluster analysis is also applied to the intermittency parameter, comparing in this case, vectors of 8 components, each of these being the p_0 value for the 8 timescales λ=1,2,4,8,16,32,64,128.

3 Results and Discussion

Results are presented relatively to gauge R7, for brevity. This station has been selected because of its localization in the strict city center, its installation in perfect meteorological conditions on the ground, and the existence of former historical rainfall records. Results for the other gauges are qualitatively similar to those shown for R7.

3.1. Empirical BDCs distributions

BDCs histograms are calculated using the non-overlapping moving window algorithm, and plotted in Fig. 7 for gauge R7 and a sequence of analyzed breakdown times. It is clearly visible that despite the randomization procedure removes pronounced peaks of histograms at certain specific BDC values, like 0.5 or 1/3, 2/5, 1/4 and 2/3, 3/5, 3/4 respectively (Fig. 5), the plots especially for timescales exceeding λ=8 remain still irregular, reducing the possibility of identifying the proper theoretical distribution. Visible irregularities of BDC histograms increase with increasing timescales, which is an obvious effect of decreasing datasets and thus decreasing populations of calculated BDC values not allowing to produce histograms of fine bins resolution. Similarly, Fig. 8 reports the distributions of BDC calculated through the overlapping moving window algorithm. The comparison between Fig.7 and Fig.8 shows how the change of algorithm from non-overlapping to overlapping moving window has brought to evident smoothing of BDC histograms especially for larger timescales, but occurring also at small timescales. Note that the smoothness of BDC histograms in Fig. 8 is comparable with the quality of BDC histograms showed by Licznar et al. (2011b) for German gauges, derived using non-overlapping moving window algorithm for much longer precipitation time series ranging from 27 to 46 years of continuous records. The introduction of the overlapping moving window algorithm allowed for the fitting of MCM parameters in the case of Warsaw gauges with the availability of extremely short time series (say 2 years long). The overall acceptance of overlapping moving window algorithm implementation, also for short rainfall time series is discussed in paragraph 3.3.

3.2. Theoretical BDCs distributions and their evolution along timescales

In Fig. 8, we report also the fitted theoretical distributions (2N-B distribution in solid red curves, and Beta distribution in blue dashed lines) for each timescale considered. The visual comparison clearly indicates a better fit of 2N-B (or N-B in some cases) distribution for timescales smaller than λ=64. In Fig.8, it is possible to see how the distribution with the best fit changes from a Beta distribution (B) at λ=128, to a joined double Normal-Beta distribution (2N-B) for the smallest value of λ, through a joined Normal-Beta distributions (N-B). This is in agreement with previous studies by Licznar et al. (2011a,b). This observation is supported by higher values of log-likelihood for 2N-B distribution (or the simplified N-B) in comparison to the Beta distribution (Tab. 1). These differences are in the range of thousands, and even after accounting for the number of model parameters, the AIC for 2N-B (or the simplified N-B) distributions are much smaller (or equal) the one of Beta distributions, confirming the visual result given in Fig. 8. Based on this, we prefer the 2N-B distribution respect to the Beta distribution, except for the case λ=128. Analyzing the data reported in Tab. 1, it is worth to notice the systematic increase of sample size *n* increasing the timescale.

From the practical point of view a rapid increase in the number of BDCs, equal or close to 0.5, decreasing the timescale should be expected, as a symptom of enclosing a limit of the precipitation temporal variability in a point by accessible instruments. The precipitation averaging over some small area of orifice and time intervals is inevitable for gauges, thus for small timescales most of small scale precipitation variability remains undetected and smoothed leading to an over-representation of constant precipitation time intervals. From the theoretical point of view, it should be noticed that bounded cascades allow the multiplicative weights (or precisely their distributions) to depend on the cascade level and converge to unity

as the cascade proceeds. As a consequence, the simulated random process becomes smoother on smaller timescales (Lombardo et al. 2012), which in general mimics the dynamics of precipitation collected by gauges. In other words, as it was postulated by Marshak et al. (1994), Menabde et al. (1997) and Harris et al. (1998) the variance of weights reduces with every descending cascade level. As a simple extension of this rule, the increasing frequency of weights at the central part of their distribution plots has to be observed. The increase in the number of BDCs equal or close to 0.5 with decreasing timescale is well illustrated by empirical histograms at well-known pioneering contributions to MCM applications for rainfall time series disaggregation, published by Olsson (1998), Menabde and Sivapalan (2000) and Güntner et al. (2001). Quite recently, this behavior was also proved to be rainfall intensity dependent by Rupp et al. (2009).

For each analyzed timescale, we have estimated the parameters of 2N-B probability distribution (or its simplifications N-B and B): p_1, p_2, a, σ_1 and σ_2. Table 2 gives the values for gauge R7 with their 95% confidence limits. A good visual fit of empirical BDC distributions in Fig. 8 corresponds to quite narrow 95% confidence limits of the fitted parameters (mostly invisible on Fig. 9 plots). The 95% confidence limits are not exceeding few percent of the estimated values, with the sole exception of parameter p_1 for λ=4, where the differences range up to 27%. Additionally, the scale parameters of Normal distributions, σ_1 and σ_2, appear to be constant among analyzed timescales, not only for gauge R7, but also for the other Warsaw gauges.

The variability of p_1, p_2, a with λ is presented in Fig. 9 for gauge R7. A systematical decrease of p_1 down to 0 increasing the timescale is observed, denoting a decreasing importance of the first Normal within the 2N-B distribution. An opposite systematical increase of p_2 up to 1 increasing the timescale is observed, denoting a decreasing importance

of the second Normal within the 2N-B distribution. The evolution of the Beta parameter *a* shows a fast reduction with below 1 values noticed for the smallest scales, yielding the change of Beta distribution shape from convex to concave. At larger timescales, the reduction of *a* is hardly visible with the sole exception of λ=128. Figure 9 shows the variability of intermittency parameters p_0 with timescale λ. For all of them, the values of p_0(*LEFT*) match the values of p_0(*RIGHT*), which is in good agreement of previous studies of Molnar and Burlando (2005) and Licznar et al. (2011a, 2011b). Systematical increase of p_0 with λ is observed with the sole exception of some small drop at λ=128.

3.3. Performance of the overlapping moving window algorithm

The performance of the overlapping moving window algorithm was investigated in detail at gauge R7, where a 25-year long time series at 15-min resolution was available. We calculate the parameters of 2N-B distribution for the hierarchy of subdaily timescales λ*'* relatively to the following 5-year periods: 1983-1987, 1988-1992, 1993-1997, 1998-2002 and 2003-2007 (indicated in the next with the roman numbers I,II,..,V respectively) and the whole 25-year dataset (indicated in the next with case A) using the overlapping moving window algorithm. In addition, we calculate the parameters of 2N-B distribution also using the classical non-overlapping moving window algorithm over the whole 25-year dataset (indicated in the next as case B). The results are shown in Fig.s 11-13.

In general, the selected probability distribution was a Beta for the largest timescales (λ*'*=16, 32), a N-B for λ*'*=2,4,8, and a 2N-B distribution for λ*'*=1 (with the only exception of the period IV). The above listed timescales λ*'* are not compatible with timescales λ, however

493 transposing them on a coherent time axis leads to the conclusion that characteristic transitions
494 from Beta to N-B and 2N-B distributions occurred at approximately the same time ranges.
495 The estimated parameters σ_1 and σ_2 appeared to be constant among analyzed timescales, and
496 equal to 0.0646 and 0.1363 respectively. These values were very close to those reported in
497 Tab. 2. Fig. 11 shows the estimates of p_1, for λ'=1, with a variability in the range 0 -- 0.058
498 for the 5-year periods I-V. At the same time, the 95% confidence limits of p_1 overlap partially
499 one on the other, and with values estimated for cases A and B. Confidence limits for periods
500 I-V are rather wide and are reduced of 50% only for cases A and B. Note that here we work
501 with 15-min time series, and not 1-min time series as before.
502 A better agreement was observed for larger timescales, as illustrated in Fig.s 12 and
503 13, with visibly narrow 95% confidence limits, but still partial overlapped one on the other.
504 For smaller timescales, larger oscillations of p_2 parameter could be observed over the periods
505 I-V, but due to wider 95% confidence limits, they overlap one on the other and with those
506 relative to cases A and B. The only exception is found for the period III at timescale λ'=1.
507 For parameter *a* and λ'=1, 95% confidence limits for all calculations overlap with the
508 only exception of period V, having slightly lower values. For λ'=2 and λ'=4, mutual overlay
509 of 95% confidence limits was noticed. Passing to λ'=8 and λ'=16, the overlapping among all
510 pairs of periods from I to V was not always present, but present with 95% confidence limits
511 drawn for case B. For λ'=32, 95% confidence limits for periods I-V and case A were
512 extremely narrow.
513 Results reported above suggest good repeatability of BDCs distributions calculated
514 during all periods, which finds its graphical confirmation in Fig. 14, with the only exception
515 of period II and timescale λ'=1. Probably this could be explained by the poor performance of
516 newly proposed overlapping moving window algorithm applied to low time resolution of the

517 original time series. Reported results undoubtedly should be verified on other much longer
518 time series of better resolution like for example the 10-min time series collected at Uccle,
519 Belgium (Willems 2013).

520 As additional check of the overall performance of the applied techniques (i.e., the
521 randomization procedure, the overlapping moving window algorithm and the 2N-B
522 probability distribution), we test the performance of microcanonical cascade in disaggregating
523 the precipitation at the analyzed gauges. The MCM is used to generate 100 synthetic time
524 series at 5-min resolution on the basis of the observed 1280-min precipitation totals (similarly
525 to Molnar and Burlando 2005, Licznar et al. 2011a and b). To evaluate the goodness of
526 disaggregation, we compare the probability of zero precipitation at synthetic and observed
527 time series for all analyzed timescales. Moreover, we calculate the survival probability
528 function of nonzero synthetic precipitation amounts and compare it to the survival probability
529 function observed precipitation amounts. This analysis is limited to 5-min data, i.e. terminal
530 results of the disaggregation, most suitable for urban hydrology application. Special interest
531 on the 5-min synthetic time series was also focused by other researchers (see e.g., Molnar and
532 Burlando 2005 and 2008, Licznar et al. 2011a and b). An example of 56.3 mm event
533 disaggregation is plotted in Fig.15, for gauge R7. It should be stressed that the structure of the
534 synthetic time series is composed by uncorrelated segments like the one presented in Fig.15.
535 Thus, the synthetic time series is missing the correct autocorrelation structure of natural
536 precipitation (for detail discussion see: Lombardo et al. 2012). The expected value of the zero
537 precipitation probability, $E(p_0)$, for observed and generated series is given in Fig. 16, for
538 gauge R7. The synthetic values of $E(p_0)$ are calculated as average over 100 MCM
539 disaggregations. The differences in terms of $E(p_0)$ between observed and simulated are
540 negligible (see Fig. 16). In addition, for comparison, we give also the synthetic values of $E(p_0)$
541 for gauges R15 and R25.

542 Fig. 17 shows the comparison between observed and simulated survival probability
543 function of rainfall amount at 5-min, for gauge R7. In Fig. 17, for gauge R7, we report the
544 empirical survival probability function for a synthetic series out of 100, and the averaged
545 function using all the generated series. In addition, for comparison, we give also the averaged
546 survival functions for gauges R15 and R25. At first glance, highest rainfall intensities drawn
547 in Fig. 17 show strange behavior manifested by constant exceedance probability above a
548 given precipitation threshold. This is especially pronounced for observed or synthetic series
549 from a single MCM run. This is due to the very short rainfall time series used for the
550 calculation of survival probability functions. According to multifractal theory, singularities in
551 small dataset are very rare. Highest rainfall intensities as singularities are very rare in 2-year
552 long series. The behavior of both the synthetic functions for gauge R7 in Fig. 17 is very
553 similar, with the sole exception of the extended and smoothed tail of the averaged function
554 plot. Both the synthetic functions are placed above the observed function. This displacement
555 reveals over-prediction of 5-min precipitation depths, particularly at the range of intensities
556 from 0.3 mm/5min to about 2.0 mm/5min. It should be noticed, that the magnitude of
557 dissimilarities between synthetic and observed survival functions for gauge R7 did not exceed
558 the ones reported in other works, see e.g., Molnar and Burlando (2005), Licznar et al.
559 (2011a,b). In comparison, the magnitude of dissimilarities between observed survival
560 probability for gauge R7 and synthetic (average) survival probability function for other
561 gauges R15 and R25 was much more pronounced.

562 **3.4. Cluster analysis results and their interpretation**

563

564 Dendrograms summarizing the results of the cluster analysis for BDC histograms are
565 produced for each timescale, and reported in Figs 18 and 19 only for λ=1 and λ=128,

566 respectively. Results for the first four timescales, i.e. λ= 1,2,4,8, are unsurprising and easy to
567 be interpreted. All Warsaw gauges are grouped in a single cluster with similar shapes of BDC
568 histograms. For all Warsaw gauges their interconnection on the dendrogram is placed at the
569 level of binding distance equal to about 0.5. Only R25 seems to be characterized by slightly
570 different pattern of BDC histogram. However, gauge R25 has a behavior, which is still much
571 closer to other Warsaw gauges, rather than the behavior of the other cities considered. For
572 example, at λ=1, gauge R25 is merged into Warsaw gauges cluster at an Euclidean distance
573 equal to 0.81, whereas the same occurs for Kielce (the closest considered Polish city) gauge at
574 the Euclidean distance equal to 1.07. For other timescales, λ= 2, 4, 8, gauge R25 merges the
575 cluster of Warsaw gauges at quite similar Euclidean distances: 0.89, 0.83 and 0.81
576 respectively.

577 The dendrogram for λ=128 is given in Fig. 19, being representative of timescales
578 λ=16,32,64,128. From Fig.19, it is possible to see the departure of gauge R15 from the cluster
579 of other Warsaw gauges. The position of gauge R15 is isolated from other Warsaw gauges
580 and its Euclidean distance from the closest one is large, and increases increasing the
581 timescale; it is equal to 1.80, 3.19, 3.88, and 8.03 respectively for λ=16, 32, 64 and 128.
582 Simultaneously, the Euclidean distance from the cluster of Warsaw gauges to the nearest
583 neighbor does not exceed 0.90, 1.00, 1.40 and 1.89 respectively for λ=16, 32, 64 and 128.

584 This last observation puts in evidence that in general the variability of BDC shapes,
585 among Warsaw gauges, increases increasing the timescale. It may partly be explained by the
586 already mentioned evolution of histogram shapes, and the replacement of 2N-B distribution
587 by less centered N-B and finally B distribution characterized by a higher variance of BDC. In
588 the specific case of gauge R15, its BDC histograms for the largest timescales are boldly
589 concave (not shown for brevity) and their shapes are becoming similar to Beta symmetrical

590 distributions parameterized by very small values of a: 0.76, 0.64, 0.54, and 0.45 respectively
591 for λ= 16,32, 64, and 128.

592 As last step, we used the cluster analysis to investigate the variability among the
593 gauges, in terms of the intermittency parameter p_0 considered as a vector having as the 8
594 components its values in correspondence of the considered timescales. Results are given in
595 form of dendrogram in Fig. 20. With respect to p_0, all Warsaw gauges form one single chain-
596 like cluster. Three gauges in the cluster, namely R14, R25 and R15, are characterized by the
597 largest distances from the nearest neighbor with Euclidean distances equal to: 0.079, 0.064
598 and 0.0614 respectively. The distance of gauges R15 and R25 from the other stations in
599 cluster is similar to observations made for Fig.s 18 and 19. A possible, but not certain,
600 explanation for gauge R14 could be its location close to gauge R15, in a weak-developed part
601 of the city.

602 Unfortunately, we do not have access to other meteorological data to compare our
603 results with other local climate conditions. To our knowledge, studies about microclimate or
604 local turbulence were not conducted for Warsaw. However in our opinion, the anomalous
605 behavior of gauges R15 and R25 does not originate from random errors due to gauges
606 installation. As it was mentioned before, all gauges were installed in very good conditions,
607 and R15 was an airport gauge. A plausible explanation of the anomalous behavior of gauges
608 R25 and R15 could be found in its location. Gauge R25 location is on south-east suburban
609 area, in the close vicinity of forested area and Vistula river valley. This specific suburban area
610 is also most frequently a place for the development of local convection processes (prof. S.
611 Malinowski, personal communication, 2013). The anomalous behavior of gauge R15 seems to
612 arise from its specific location on the ground of the Warsaw airport. In the neighborhood of
613 the instrument there are no high buildings and trees and the ground is covered only by short
614 cut grass. The local atmospheric turbulence conditions, additionally influenced by taking off

and landing aircrafts could have favored the different behavior of this station. In general, gauges R15 and R25 are the only instruments, installed outside the areas of urban fabric (Fig. 1) in rather rural conditions of surrounding green areas. The suburban location of these gauges connected with direct green surrounding reduces, or even minimalizes to zero, urban heat island effects. Peng et al. (2011) investigated the surface urban heat island intensity across 419 global big cities (including Warsaw city). These authors showed that the distribution of daytime surface urban heat island intensity correlates negatively across cities with the difference of vegetation fractional cover, and of vegetation activity, between urban and suburban areas. Kłysik and Fortuniak (1999) for the second big city of Poland, Łódz (about 120km south-west) comparable to Warsaw flat topography, found the occurrence of the urban heat. According to statistics calculated over many years, in two stations one in center and one in airport, over 80% of nights were characterized by a surplus heat in town, amounting 2-4°C, and sporadically to 8°C and more. Once more for Łódź, Fortuniak et al. (2006) confronted the data from two automatic stations: one urban and one rural. They found the relative humidity to be lower in the town, sometimes by more than 40%, and water vapour pressure differences to be possibly either positive (up to 5 hPa) or negative (up to -4 hPa). Air temperature differences between the urban and rural station exceeded 8°C. It could be that similar processes occur in Warsaw and affect local precipitation dynamics, and gauges R7 and R15 and R25. As consequence, statistics of synthetic time series vary visibly in Figs. 16 and 17. However, the significance of these differences should be studied in more details in the future.

4 Conclusions

Owning in mind the simplicity of microcanonical cascade generators retrieval from observational data, we proposed to use this technique for the local variability of very short precipitation time series within an urban monitoring network.

639 We considered a network of 25 gauges deployed in Warsaw city (Poland) over an area
640 of 517.2 km^2. An attempt was made to define the generators of a MCM applicable for
641 producing 5-min time series, as requested by urban hydrologists, through the disaggregation
642 of quasi-daily precipitation totals. We showed that smooth distributions of BDC are possible,
643 for all analyzed timescales, even in case of limited length of time series, which in our case
644 slightly exceeded 2 years only. This was made possible by the implementation of a
645 randomization procedure and the use of an overlapping moving window algorithm for the
646 calculation of BDCs.

647 The correctness of the overlapping moving window algorithm is checked using
648 additional 15-minute rainfall time series, 25-year long, at gauge R7. The algorithm is
649 implemented for a hierarchy of subdaily timescales, and separate 5-year periods. The results
650 of BDC calculations are compared to those obtained using all 25 years of data with both
651 overlapping and non-overlapping moving window algorithms. Despite the coarse resolution of
652 data, and winter time gaps in the series, the results show a good agreement of BDC
653 distributions calculated over the different periods, suggesting the correctness of the
654 overlapping moving window algorithm, at least in central Poland.

655 To adequately describe the shapes of BDC histograms, we have implemented a special
656 joined probability distribution, 2N-B, assembled from 2 Normal distributions and 1 Beta
657 symmetrical distribution. A systematical evolution of BDC histograms from joined double
658 Normal-Beta distributions (2N-B), through joined Normal-Beta distributions (N-B) up to Beta
659 distributions (B) was observed increasing the timescale. To test the use of more complicated
660 models alternative to the classical Beta distribution, we suggested the Akaike information
661 criterion (AIC).

662 To check all the applied techniques (i.e., the randomization procedure, the overlapping
663 moving window scheme and the 2N-B distribution), MCMs were used to disaggregate 1280-

664 min precipitation into 5-min time series. The quality of the generated series was checked
665 comparing the statistical properties of these with the ones of observed series. In particular, we
666 compared probabilities of zero precipitation and the survival probability functions of non-zero
667 5-min precipitation amounts, for the considered timescales, with agreement comparable to
668 previous studies made in Switzerland, Germany and Poland.

669 As main part of this study, we have conducted an intercomparison of BDC histograms
670 among the 25 Warsaw gauges, and considering as a term of reference also other 6 gauges
671 located in Poland and Germany. The intercomparison was made, scale-by-scale, by means of
672 cluster analysis. Resulting dendrograms for small timescales (i.e. λ=1,2,4,8) revealed rather
673 small variability of BDC histograms among all Warsaw gauges in comparison to the
674 variability exhibited with respect to the other external gauges. Only gauge R25 seems to be
675 characterized by a slightly different pattern. It might originate from the specific gauge
676 location on the city boundary, in the vicinity of forested areas and Vistula river valley.

677 Dendrograms obtained for large timescales (i.e. λ=16, 32, 64, 128) also delivered a
678 general picture of similarity among Warsaw gauges, with the very clear exception of gauge
679 R15. To our best knowledge a possible explanation of this was its installation on the ground
680 of the Warsaw airport, strongly man-modified and with local turbulence conditions. In
681 addition, R25, R15, and R14 were also identified as gauges presenting slightly different
682 behavior in terms of the intermittency parameter p_0.

683 As final remarks, we can affirm that MCMs combined with cluster analysis could be
684 used as a tool for the assessment of the spatial variability of local precipitation patterns among
685 a group of gauges. This framework could be effectively implemented even in case of very
686 short observational series thanks to the proposed overlapping moving window algorithm. We
687 believe that the use of this algorithm could increase the development and use of MCMs in
688 urban hydrology. At the same time, we are fully aware of the inherent MCM limitations in the

quality of rainfall disaggregation and the necessity of additional verifications of the overlapping moving window algorithm for other gauges with longer and better quality observational time series. From current engineering needs in urban hydrology, it is enough to use only one fitted MCM for the precipitation time series disaggregation in Warsaw city. We suppose that this result could be valid even in larger urban areas, but the verification is necessary. We dissuade from the cascade generation fitted on precipitation time series collected at instruments located out of the city center in unrepresentative sites, like in our case, the ground of the airport. We question the practice of using gauges from airport for urban hydrology. We recommend further research to assess the influence of the local conditions on BDC histograms to find more clear explanations of anomalies. We also recognize the necessity of further tests on other cities and precipitation monitoring networks, especially in case of cities with complicated orography and presence of hydrological networks.

Acknowledgements

This project was financed by the Polish National Science Centre (NCN) funds allocated on basis of decision no 2011/03/B/ST10/06338. It was realized as a part of scientific project: "Spatio-temporal analysis and modeling of urban precipitation field." Precipitation data was provided by the Municipal Water Supply and Sewerage Company (MWSSC) in Warsaw, Poland. Authors also acknowledge the three anonymous reviewers for their suggestions and comments.

References

Ahrens, B.: Rainfall downscaling in an alpine watershed applying a multiresolution approach, J. Geophys. Res., 108, 8388, doi:10.1029/2001JD001485, 2003.

Arbeitsblatt DWA-A 117.: Bemessung von Regenrückhalteräumen. Deutsche Vereinigung für Wasserwirtschaft, Abwasser und Abfall e. V., Hennef, 2006.

Appendix B. Report on Approaches to UWWTD Compliance in Relation to CSO's in major cities across the EU. Thames Tunnel Needs Report, 2010.

Berne, A., Delrieu, G., Creutin, J.D. and Obled, C.: Temporal and spatial resolution of rainfall measurements required for urban hydrology. J. Hydrol., 299(3-4), 166-179, doi: 10.1016/j.jhydrol.2004.08.002, 2004.

Cârsteanu, A., and Foufoula-Georgiou, E.: Assessing dependence among weights in a multiplicative cascade model of temporal rainfall, J. Geophys. Res. 101, D21, 26363-26370, doi: 10.1029/96JD01657, 1996.

De Michele, C., Salvadori, G., Vezzoli, R. and Pecora, S.: Multivariate assessment of droughts: Frequency analysis and dynamic return period, Water Resour. Res., 49, 6985–6994, doi:10.1002/wrcr.20551, 2013.

EN 752, Drain and sewer systems outside buildings, 1997.

Fortuniak, K., Klysik, K., and Wibig, J.: Urban–rural contrasts of meteorological parameters in Lodz. Theor. Appl. Climatol., 84, 91–101, doi: 10.1007/s00704-005-0147-y, 2006.

Gires, A., Onof C., Maksimovic C., Schertzer D., Tchiguirinskaia I., and Simoes N.: Quantifying the impact of small scale unmeasured rainfall variability on urban hydrology through multifractal downscaling: a case study. J. Hydrol., 442–443, 117–128, doi: 10.1016/j.jhydrol.2012.04.005, 2012.

Gires, A., Tchiguirinskaia, I., Schertzer, D. and Lovejoy, S.: Multifractal analysis of an urban hydrological model on a Seine-Saint-Denis study case. Urban Water J., 10(3), 195-208, doi: 10.1080/1573062X.2012.716447, 2013.

Górski J.: Analysis of Precipitation Time Series for Needs of Urban Hydrology on Example of Kielce City. PhD thesis (in Polish), Kielce University of Technology, 2013.

Harris, D., A. Seed, Menabde M., and Austin G.: Factors affecting multiscaling analysis of rainfall time series, Nonlin. Processes Geophys. 4, 3, 137-156, doi: 10.5194/npg-4-137-1997, 1997.

Hingray B., and Ben Haha, M.: Statistical performances of various deterministic and stochastic models for rainfall series disaggregation. Atmos. Res., 77, 152– 175, 2005.

Kłysik, K., and Fortuniak, K.: Temporal and spatial characteristics of the urban heat island of Łódź, Poland. Atmos. Environ, **33**, 3885–3895, 1999.

761 Koutsoyiannis, D.: Rainfall disaggregation methods: Theory and applications, in: D. Piccolo
762 and L. Ubertini (eds.), Proc. Workshop on Statistical and Mathematical Methods for
763 Hydrological Analysis, Rome, 1-23, Universitá di Roma "La Sapienza",
764 http://itia.ntua.gr/en/docinfo/570, 2003.
765
766 Lanza L., Leroy M., Alexandropoulos C., Stagi L., and Wauben W.: WMO laboratory
767 intercomparison of rainfall intensity gauges. Final report. IOM Report No. 84, WMO/TD No.
768 1304, 2005.
769
770 Larose, D. T.: Discovering knowledge in data: an introduction to data mining. John Wiley &
771 Sons, Inc., Hoboken, New Jersey, 2005.
772
773 Licznar, P.: Stormwater reservoir dimensioning based on synthetic rainfall time series.
774 Ochrona Srodowiska, 35(2), 27–32, 2013.
775
776 Licznar, P., Łomotowski, J., and Rupp, D. E.: Random cascade driven rainfall disaggregation
777 for urban hydrology: An evaluation of six models and a new generator, Atmos. Res. 99, 3-4,
778 563-578, doi:10.1016/j.atmosres.2010.12.014, 2011a.
779
780 Licznar, P., Schmitt, T. G., and Rupp, D. E.: Distributions of microcanonical cascade weights
781 of rainfall at small timescales, Acta Geophysica, 59 (5), 1013-1043, doi:10.2478/s11600-011-
782 0014-4, 2011b.
783

784 Lombardo, F., Volpi, E., and Koutsoyiannis, D.: Rainfall downscaling in time: theoretical and
785 empirical comparison between multifractal and Hurst-Kolmogorov discrete random cascades,
786 Hydrolog. Sci. J., 57(6), 1052-1066, doi: 10.1080/02626667.2012.695872, 2012.
787
788 Marshak, A., Davis, A., Cahalan, R., and Wiscombe, W.: Bounded cascade models as
789 nonstationary multifractals, Phys. Rev. E, 49,55-69, 1994.
790
791 Menabde, M., and Sivapalan, M.: Modeling of rainfall time series and extremes using
792 bounded random cascades and Levy-stable distributions, Water Resour. Res., 36(11), 3293–
793 3300, doi:10.1029/2000WR900197, 2000.
794
795 Menabde, M., D. Harris, A. Seed, G. Austin, and Stow D.: Multiscaling properties of rainfall
796 and bounded random cascades, Water Resour. Res. 33, 12, 2823-2830, doi:
797 10.1029/97WR02006, 1997.
798
799 Molnar, P., and Burlando, P.: Preservation of rainfall properties in stochastic disaggregation
800 by a simple random cascade model, Atmos. Res., 77, 1-4, 137-151,
801 doi:10.1016/j.atmosres.2004.10.024, 2005.
802
803 Molnar, P., and Burlando, P.: Variability in the scale properties of high-resolution
804 precipitation data in the Alpine climate of Switzerland, Wat. Resour. Res., 44, W10404,
805 doi:10.1029/2007WR006142, 2008.
806

807 Oke T.: Initial guidance to obtain representative meteorological observations at urban sites,
808 Instruments and Observing Methods, Report no. 81, World Meteorological Organization,
809 WMO/TD-No. 1250, 2006.
810
811 Olsson J.: Evaluation of a scaling cascade model for temporal rainfall disaggregation, Hydrol.
812 Earth Syst. Sci., 2, 19-30, DOI: 10.5194/hess-2-19-1998, 1998.
813
814 Over, T. M., and Gupta V. K.: A space-time theory of mesoscale rainfall using random
815 cascades. J. Geophys. Res., 101(D21), 26319-26331. 1996
816
817 Paulson, K.S., and Baxter P. D.: Downscaling of rain gauge time series by multiplicative beta
818 cascade, J. Geophys. Res. 112, D09105, doi: 10.1029/2006JD007333, 2007.
819
820 Peng, S., Piao, S., Ciais, P., Friedlingstein P., Ottle C., Bréon F.-M. Nan H., Zhou L. and
821 Myneni R.B.: Surface Urban heat island across 419 global big cities, Environ. Sci.
822 Technol., 2012, 46 (2), 696–703, doi: 10.1021/es2030438, 2012.
823
824
825 Robert, C.P.: Simulation of truncated normal variables, Statistics and Computing 5, 121–125,
826 1995.
827
828 Rupp, D. E., Keim, R. F., Ossiander, M., Brugnach, M., and Selker, J. S.: Time scale and
829 intensity dependency in multiplicative cascades for temporal rainfall disaggregation, Water
830 Resour. Res., 45, W07409, doi:10.1029/2008WR007321, 2009.
831

Rupp D. E., P. Licznar, W. Adamowski, and Leśniewski M.: Multiplicative cascade models for fine spatial downscaling of rainfall: parameterization with rain gauge data. Hydrol. Earth Syst. Sci., 16, 671–684, doi:10.5194/hess-16-671-2012, 2012.

Schmitt, T. G.: ATV-DVWK Kommentar, ATV-A 118 Hydraulische Berechnung von Entwässerungssystemen, DWA, Hennef, 2000.

Willems, P.: Multidecadal oscillatory behaviour of rainfall extremes. Clim. Chang., 120, 931–944, doi: 10.1007/s10584-013-0837-x, 2013.

WMO-No. 8, Guide to Meteorological Instruments and Methods of Observation. World Meteorological Organization - WMO, 2012.

Tab. 1. Values of p_1, p_2, a, σ_1 and σ_2 parameters at different timescales, for gauge R7. The values of parameters are reported in bold, whereas their 95% confidence limits are in italic.

Breakdown times	Timescale	p_1	p_2	a	σ_1	σ_2
5-10 min.	λ=1	**0.1541**	**0.3479**	**1.3350**	**0.0559**	**0.1341**
		0.1474	*0.3377*	*1.3097*	*0.0523*	*0.1300*
		0.1608	*0.3580*	*1.3604*	*0.0595*	*0.1383*
10-20 min.	λ=2	**0.0706**	**0.4036**	**1.0632**	**0.0559**	**0.1341**
		0.0644	*0.3950*	*1.0474*	*0.0523*	*0.1300*
		0.0768	*0.4121*	*1.0789*	*0.0595*	*0.1383*
20-40 min.	λ=4	**0.0212**	**0.5036**	**0.9437**	**0.0559**	**0.1341**
		0.0155	*0.4954*	*0.9325*	*0.0523*	*0.1300*
		0.0270	*0.5118*	*0.9548*	*0.0595*	*0.1383*
40-80 min.	λ=8	-	**0.6175**	**0.9484**	-	**0.1341**
		-	*0.6091*	*0.9390*	-	*0.1300*
		-	*0.6259*	*0.9579*	-	*0.1383*
80-160 min.	λ=16	-	**0.7548**	**0.9170**	-	**0.1341**
		-	*0.7494*	*0.9098*	-	*0.1300*
		-	*0.7601*	*0.9242*	-	*0.1383*
160-320 min.	λ=32	-	**0.8873**	**0.8929**	-	**0.1341**
		-	*0.8827*	*0.8873*	-	*0.1300*
		-	*0.8919*	*0.8985*	-	*0.1383*
320-640 min.	λ=64	-	**0.9797**	**0.8799**	-	**0.1341**
		-	*0.9758*	*0.8754*	-	*0.1300*
		-	*0.9835*	*0.8843*	-	*0.1383*
640-1280 min.	λ=128	-	**1.0000**	**0.7783**	-	**0.1341**
		-	*0.9973*	*0.7754*	-	*0.1300*
		-	*1.0027*	*0.7813*	-	*0.1383*

850 Tab. 2. Values of the Akaike information criterion (AIC) for 2N-B distribution (model 1) -- or its simplifications
851 N-B and B -- and Beta B distribution (model 2), and the hierarchy of analyzed timescales λ, at gauge R7.
852 Calculations were based on estimates of the maximized value of the log-likelihood function (*LL*) known sample
853 size (*n*) and number of model parameters (*k*).
854

			Model 1				Model 2				
Breakdown times	Timescale	*n*	Distr.	*k*	*LL*	AIC(M1)	Distr.	*k*	*LL*	AIC(M2)	Δ=AIC(M2) – AIC(M1)
5-10 min.	λ=1	132940	2N-B	5	48480	-96950	B	1	36307	-72612	24338
10-20 min.	λ=2	136968	2N-B	5	32272	-64534	B	1	19798	-39593	24941
20-40 min.	λ=4	144778	2N-B	5	19071	-38132	B	1	8794	-17585	20547
40-80 min.	λ=8	159272	N-B	3	11119	-22232	B	1	4464	-8927	13305
80-160 min.	λ=16	185014	N-B	3	4591.9	-9178	B	1	925	-1848	7330
160-320 min.	λ=32	230716	N-B	3	1167.3	-2329	B	1	46	-91	2238
320-640 min.	λ=64	315360	N-B	3	1543.70	-3081	B	1	1491	-2979	102
640-1280 min.	λ=128	501092	B	1	12614.40	-25227	B	1	12614	-25227	0

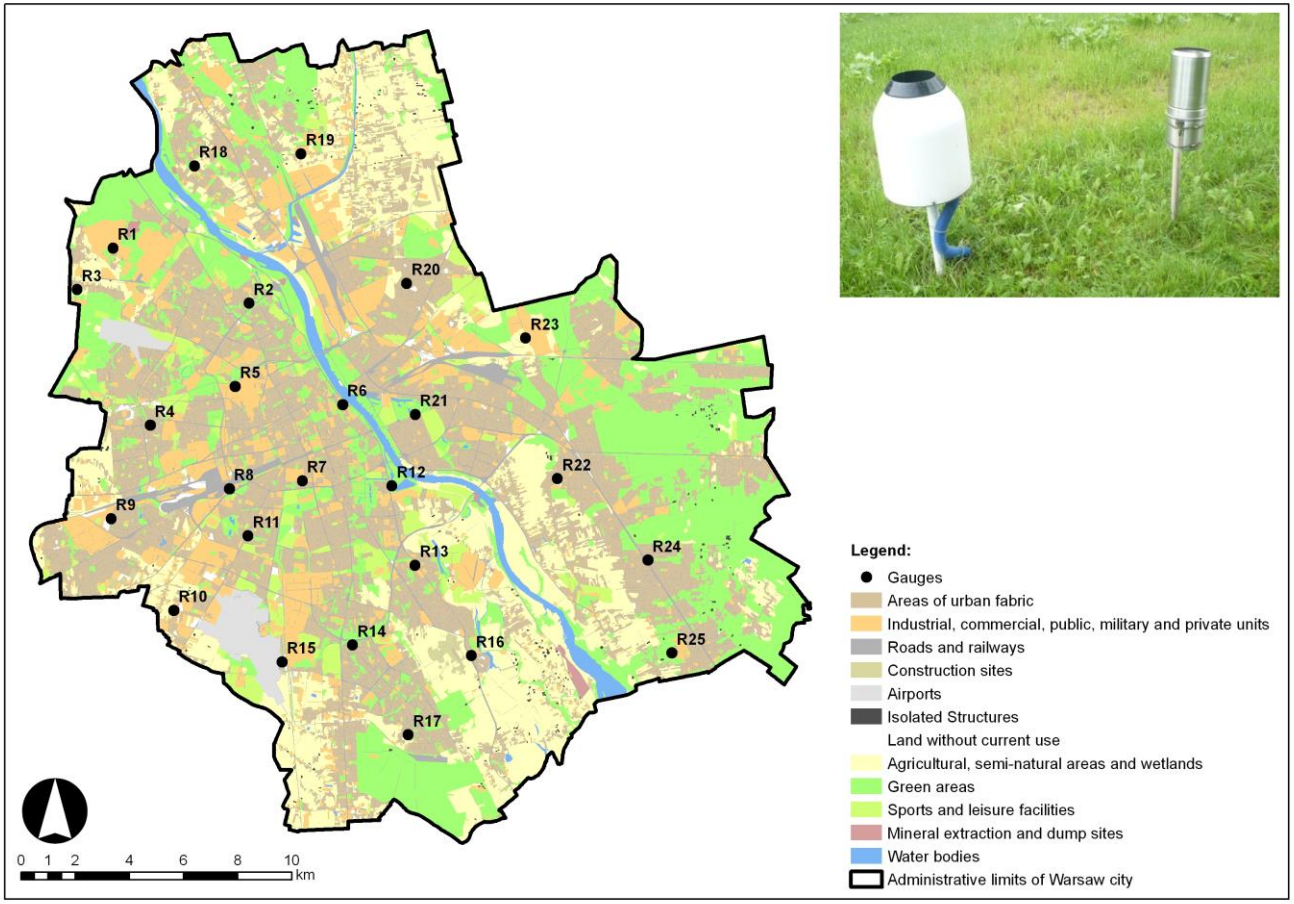

Fig. 1. Map of 25 gauges composing the precipitation-monitoring network in Warsaw. Administrative limits of Warsaw city and limits of forested areas were marked in black. The land use classification of was made through the Urban Atlas, which provides pan-European comparable land use and land cover data for large urban zones with more than 100.000 inhabitants (http://www.eea.europa.eu/data-and-maps/data/urban-atlas#tab-metadata). The average density of network is 1 instrument over 20.7 km^2. MPS weighing-type TRwS 200E gauges were accompanied with standard Hellman gauges for the routine control of daily precipitation totals.

860

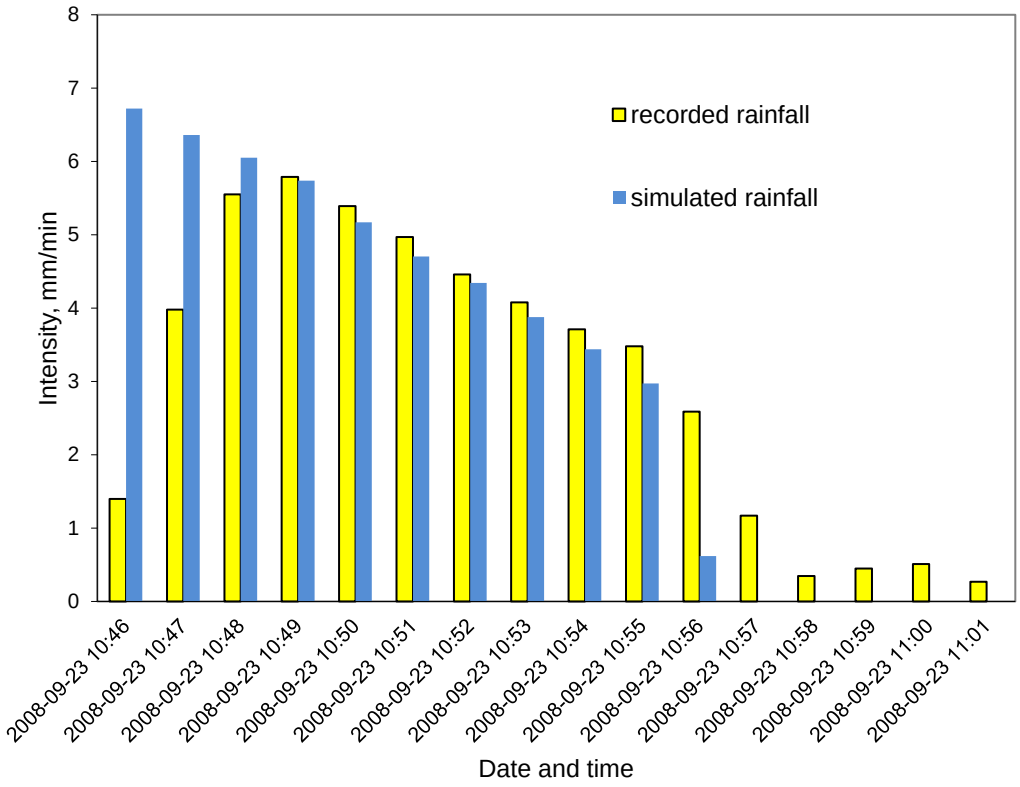

861
862 Fig. 2. Weighing-type TRwS 200E gauge during some tests (upper panel). Rainfall is simulated by means of
863 precise medical pump. Sample of test results reporting simulated and recorded rainfall depths (lower panel).
864

865
866

867
868 Fig. 3. Location of Polish and German precipitation gauges used during the comparison of Warsaw results with
869 other studies.
870

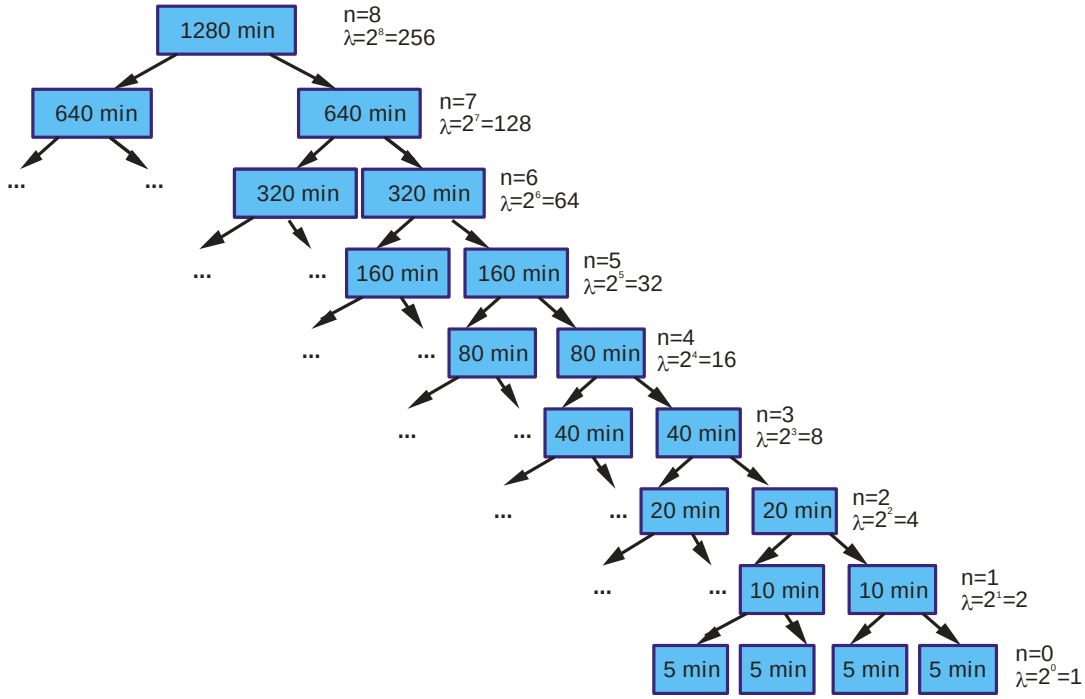

Fig. 4. Schematic diagram of developed microcanonical cascade model with branching number b=2.

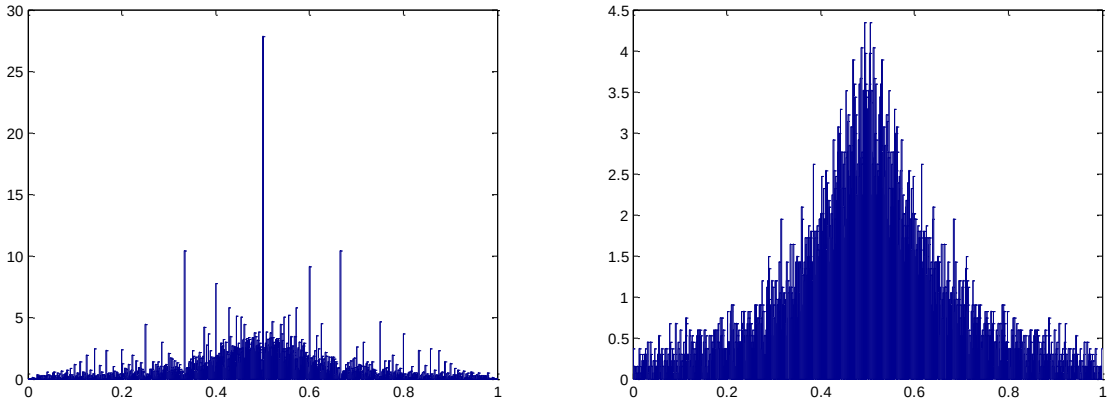

Fig. 5. Comparison of BDC histograms for gauge R7, and timescale λ=1, calculated according to the non-overlapping moving window algorithm and using original (left panel), and randomized (right panel) non-zero precipitation data. Horizontal axes show BDC range, and vertical axes the respective frequency values.

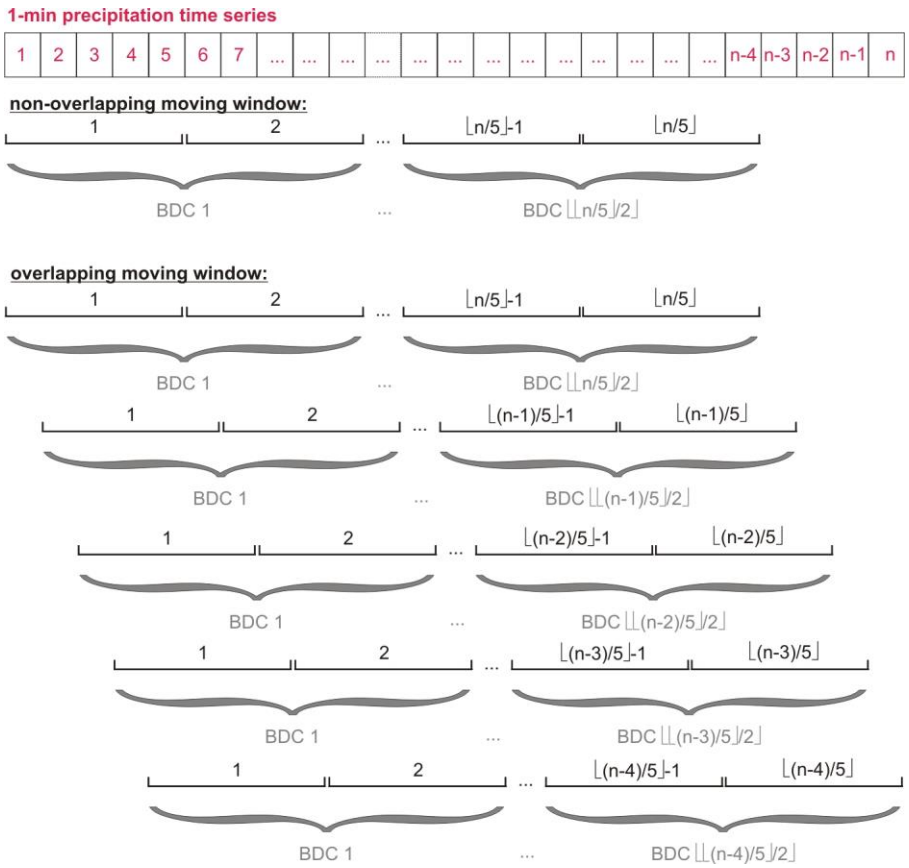

Fig. 6. Example showing differences between non-overlapping and overlapping moving window algorithms for the calculation of BDCs in case of 1-min precipitation time series and breakdown time 5-10 min. Note that $\lfloor n \rfloor$ means the integer part of *n*, where *n* is the total length of 1-min precipitation time series.

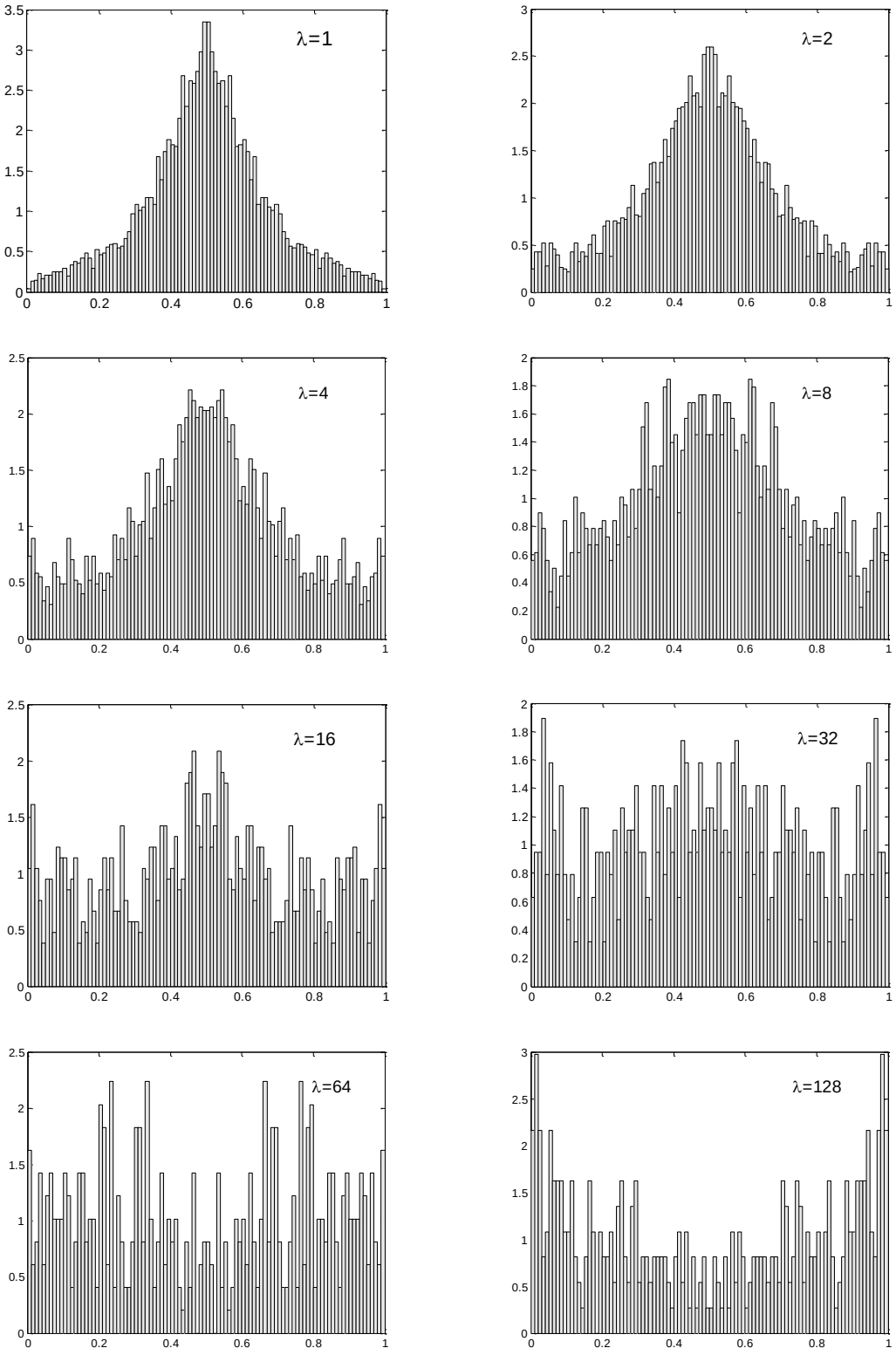

Fig. 7. Histograms of BDC values for gauge R7 calculated according to the non-overlapping moving window algorithm and based on randomized precipitation time series. Horizontal axes show BDC range and vertical axes the respective frequency values.

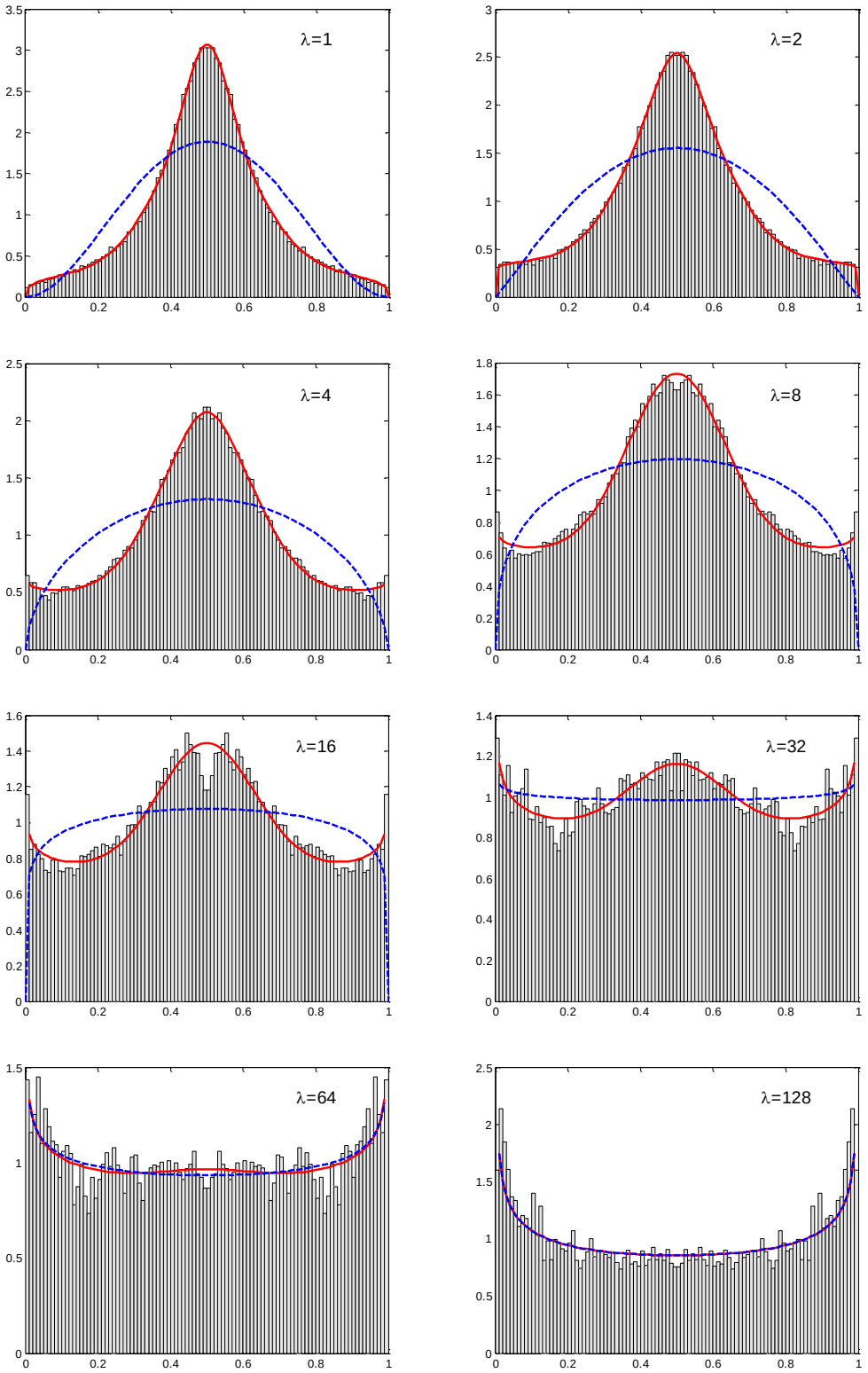

Fig. 8. Histograms of BDC values calculated according to overlapping moving window algorithm and based on randomized gauge R7 precipitation times series. Horizontal axes show BDC range and vertical axes the respective frequency values. The solid red curves represent the 2N-B probability density function, whereas the blue dashed curves the Beta probability density function.

900

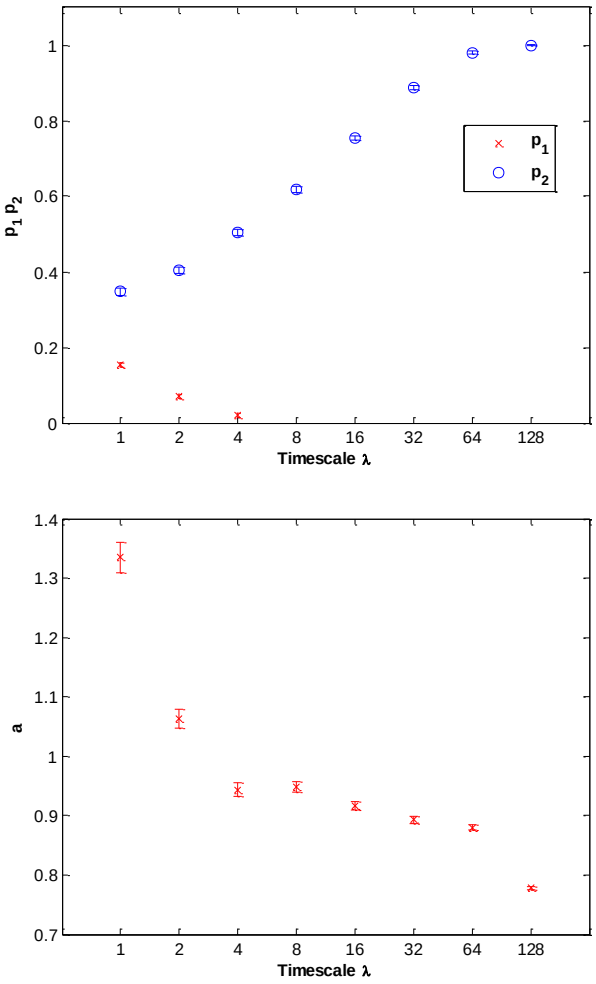

901
902 Fig. 9. Value and 95% confidence intervals of parameters of p_1, p_2 and a with λ, for gauge R7. Horizontal axes
903 are plotted at binary logarithm scale $\log_2$.
904

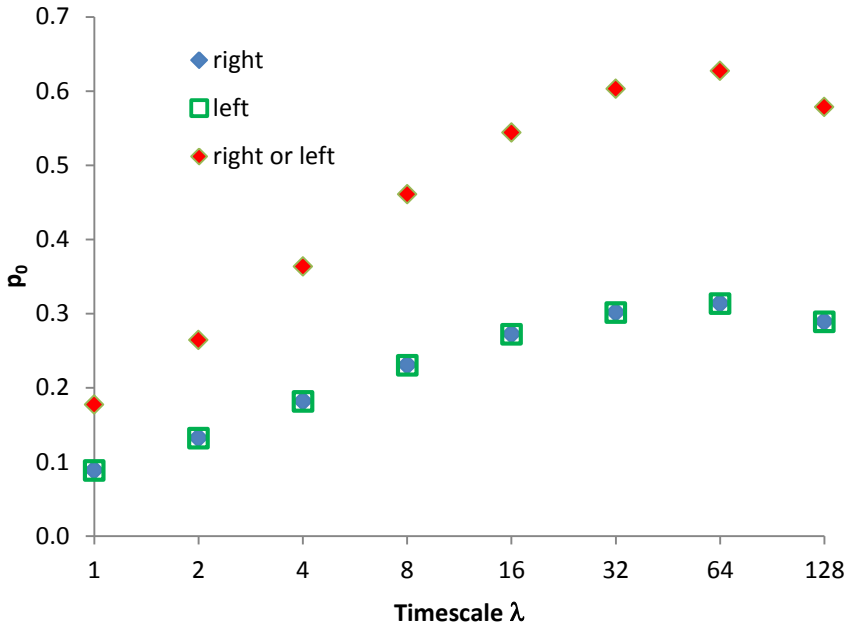

Fig. 10. Variability of the intermittency parameter p_0 with λ, for gauge R7. Horizontal axis is plotted at binary logarithm scale $\log_2$.

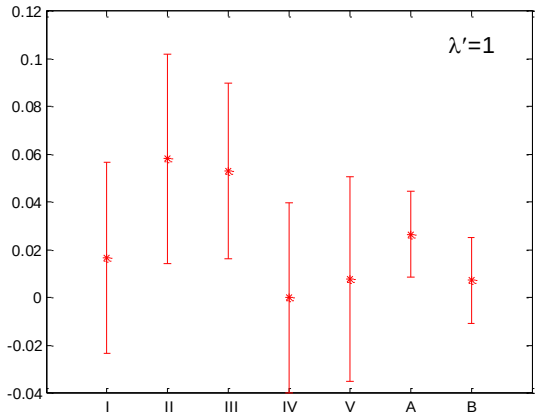

909

910 Fig. 11. Value and 95% confidence intervals of parameter p_1 at timescale λ'=1, for gauge R7. Roman numbers
911 I-V on horizontal axes indicate respectively the 5-year ranges: 1983-1987, 1988-1992, 1993-1997, 1998-2002
912 and 2003-2007. Uppercase letters A and B indicate values calculated using all 25-year range 1983-2007, and
913 non-overlapping (A), overlapping (B) moving window algorithm.
914

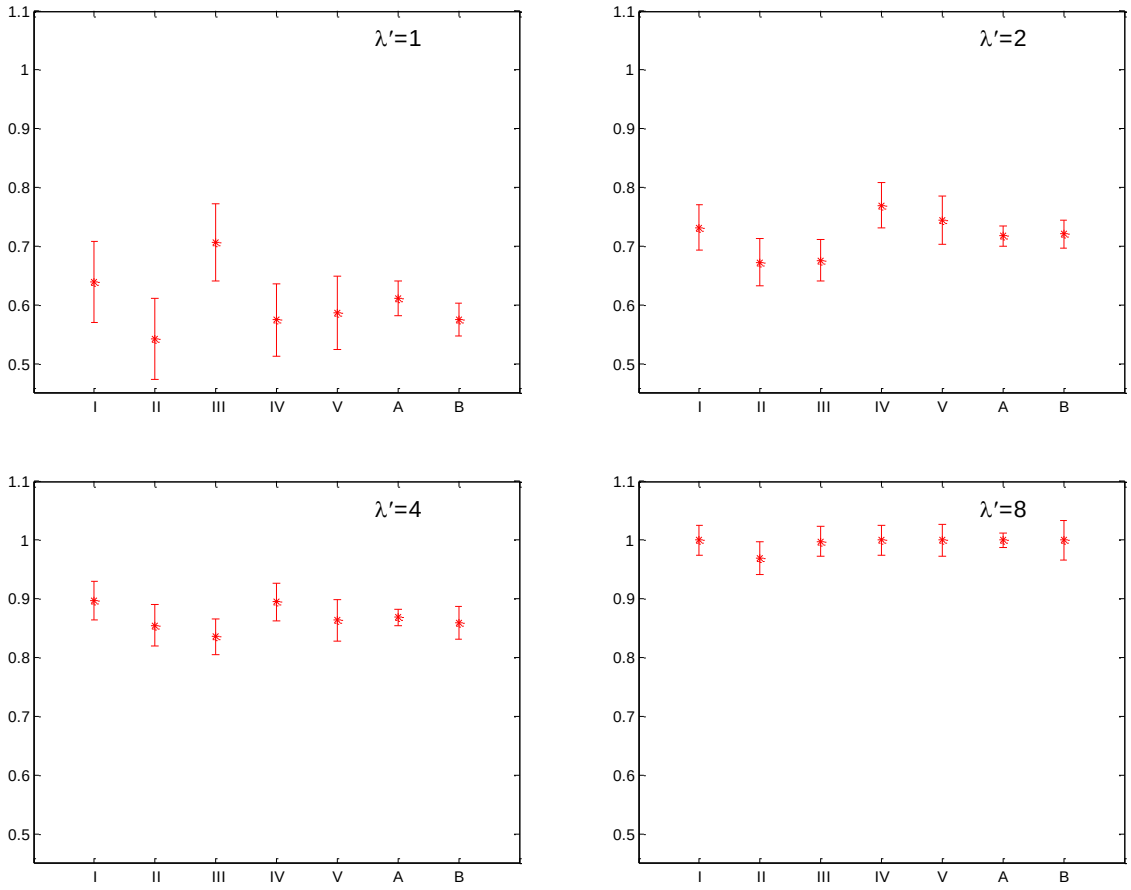

915 Fig. 12. Value and 95% confidence intervals of parameter p_2 at timescales λ'=1,2,4,8, for gauge R7. Roman
916 numbers I-V on horizontal axes indicate respectively the 5-year ranges: 1983-1987, 1988-1992, 1993-1997,
917 1998-2002 and 2003-2007. Uppercase letters A and B indicate values calculated using all 25-year range 1983-
918 2007, and non-overlapping (A), overlapping (B) moving window algorithm.
919

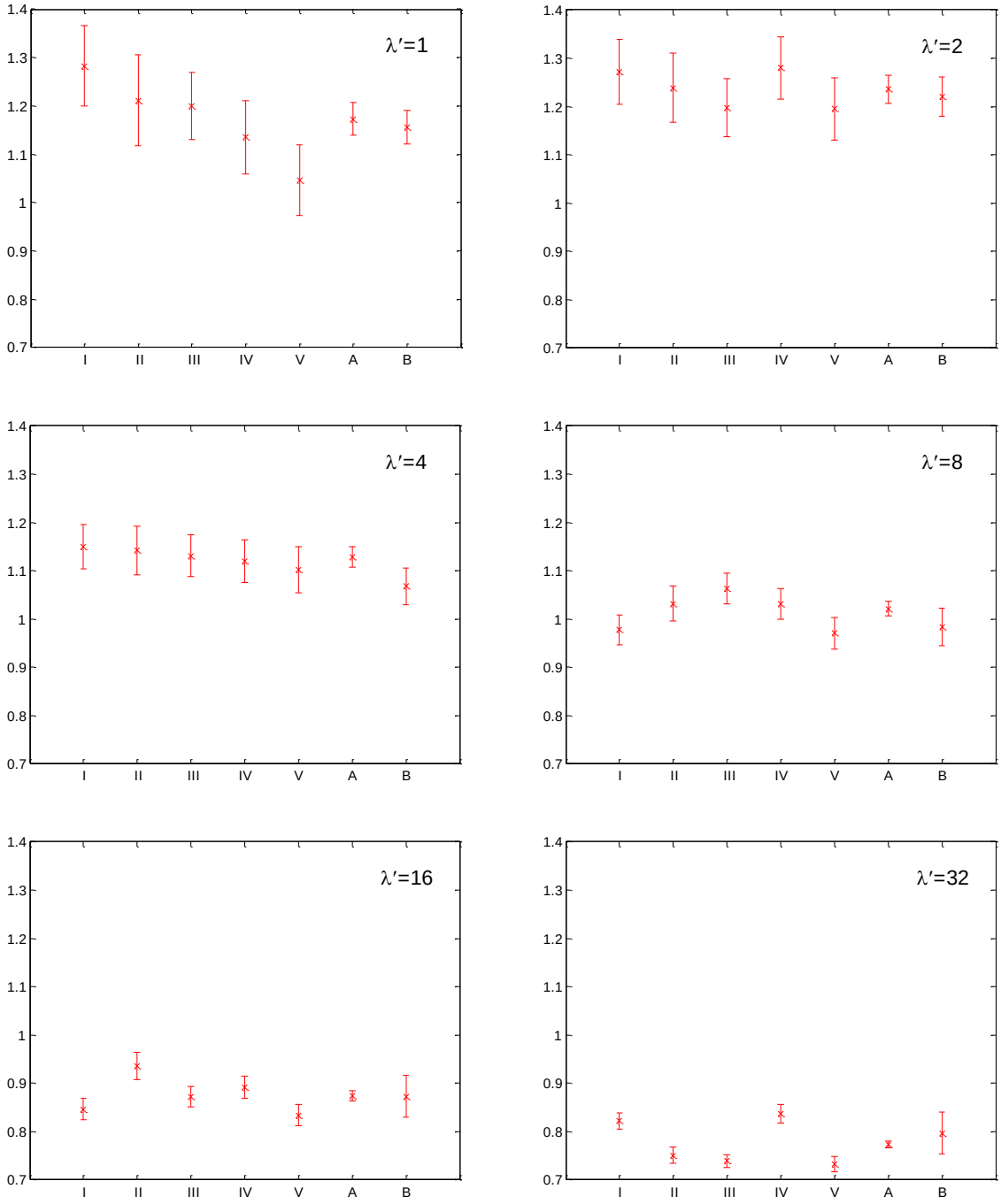

Fig. 13. Value and 95% confidence intervals of parameter *a* at timescales λ'=1,2,4,8,16,32, for gauge R7. Roman numbers I-IV on horizontal axes indicate respectively the 5-year ranges: 1983-1987, 1988-1992, 1993-1997, 1998-2002 and 2003-2007. Uppercase letters A and B indicate values calculated using all 25-year range 1983-2007, and non-overlapping (A), overlapping (B) moving window algorithm.

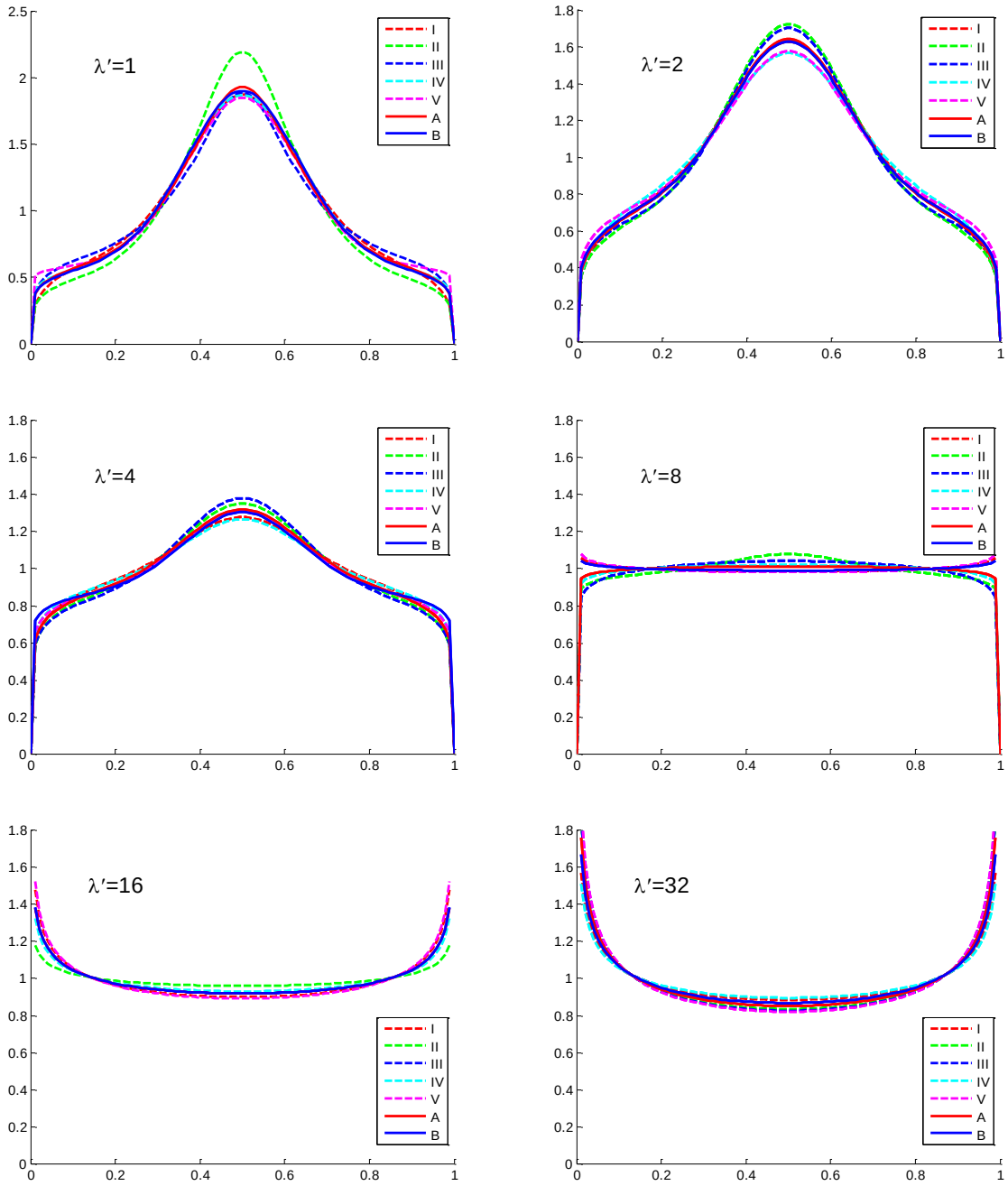

Fig. 14. Variability of fitted theoretical BDCs distributions histograms at timescales λ′=1,2,4,8,16,32, for gauge R7. Roman numbers I-V in legend indicate respectively the 5-year ranges: 1983-1987, 1988-1992, 1993-1997, 1998-2002 and 2003-2007. Uppercase letters A and B indicate results calculated using all 25-year range 1983-2007, and non-overlapping (A), overlapping (B) moving window algorithm. In all plots, horizontal axes show BDC ranges and vertical axes the frequency values.

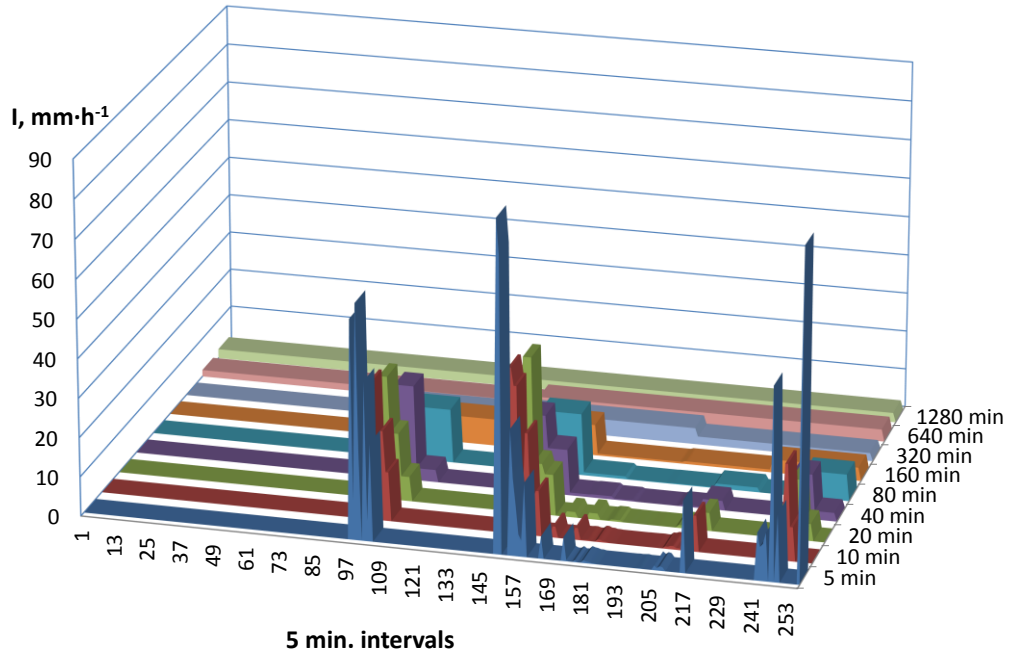

Fig. 15. An example of precipitation disaggregation of a 56.3 mm event from 1280 min to 5 min, for gauge R7.

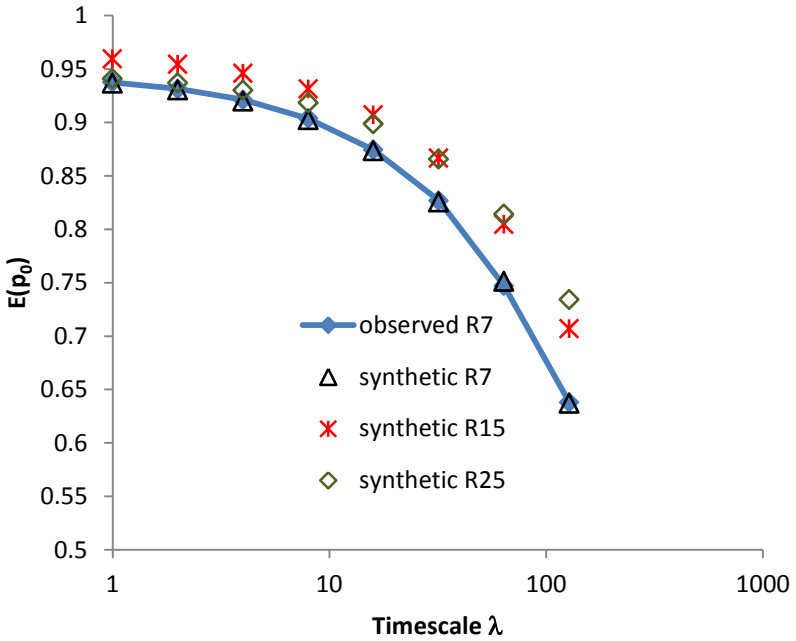

Fig. 16. Comparison between observed for gauge R7 and synthetic series for gauges R7, R15 and R25 in terms of intermittency $E(p_0)$ for the considered timescales. The values for the generated data are calculated as average of 100 disaggregation runs. The variability between runs was negligible and so is not shown here.

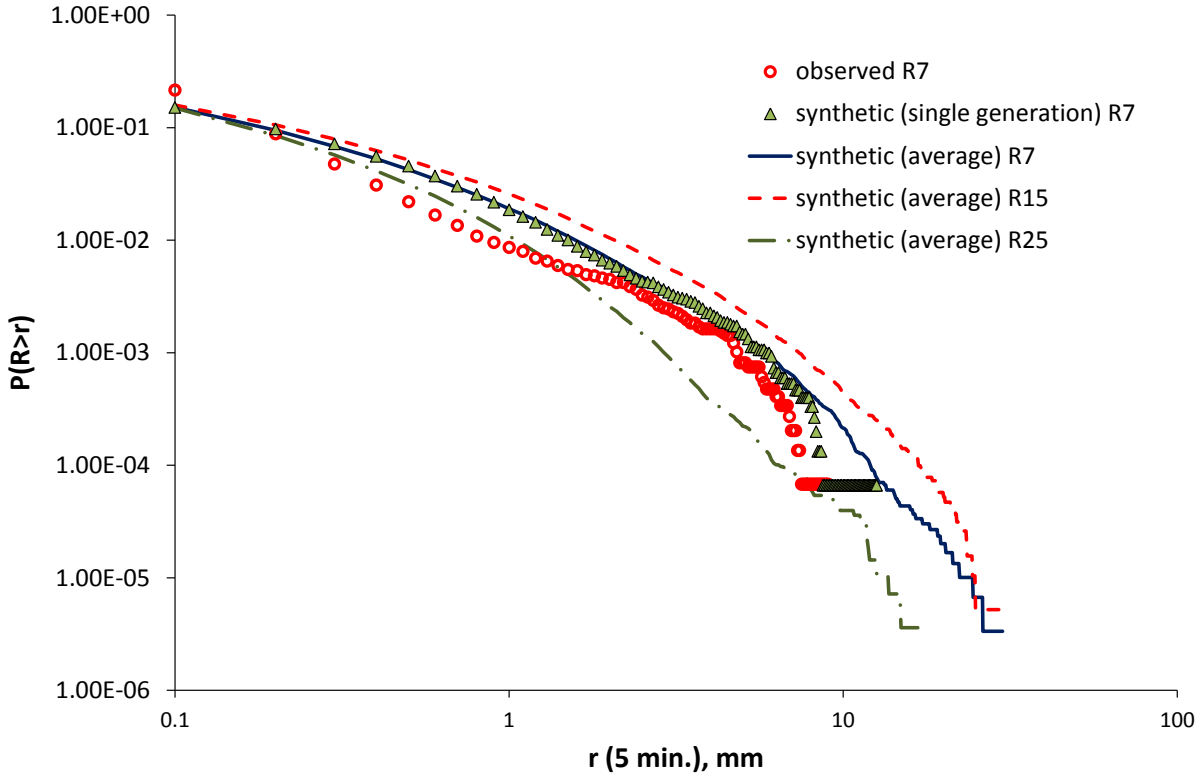

Fig. 17. The survival probability function of 5 min precipitation amounts for the observed time series (circles) and the synthetic time series (triangles) generated by the disaggregation of 1280 precipitation amounts, for gauge R7. The lines represent the average distributions calculated over the generation of 100 synthetic time series for gauge R7 and for comparison for gauges R15 and R25.

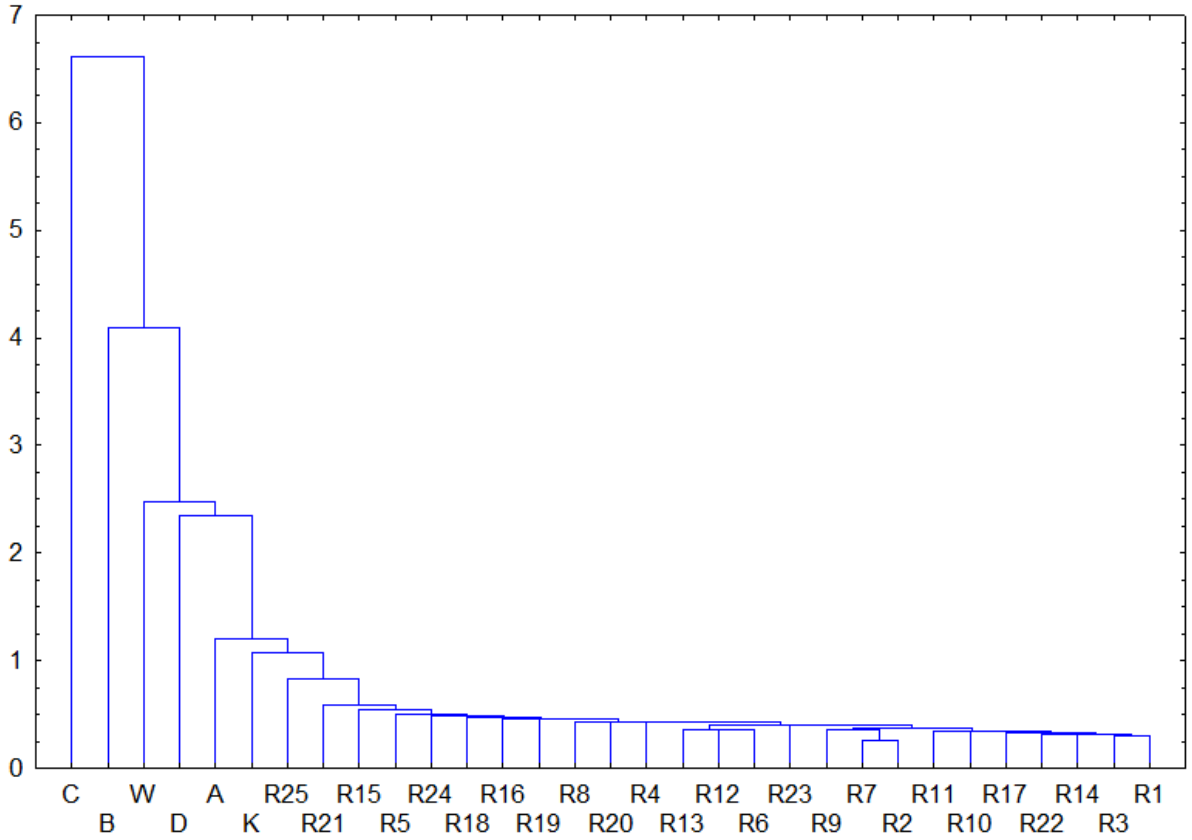

Fig. 18. Dendrogram resulting from the cluster analysis of BDC histograms for λ=1. The vertical scale shows binding distance, whereas names of gauges are given on horizontal scale (K stands for Kielce gauge, and W stands for Wroclaw).

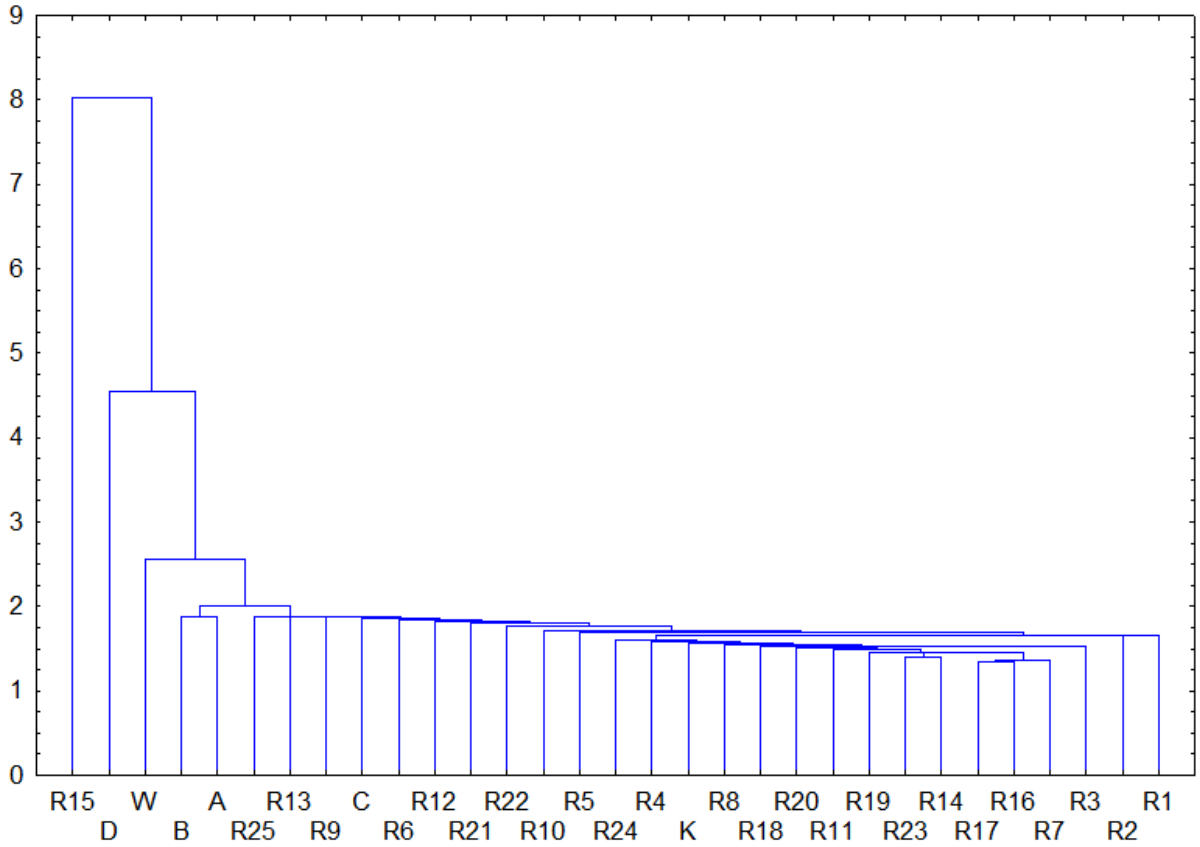

Fig. 19. Dendrogram resulting from the cluster analysis of BDCs histograms for the timescale λ=128. The vertical scale shows binding distance, whereas names of gauges are given on horizontal scale (K stands for Kielce gauge, and W stands for Wroclaw).

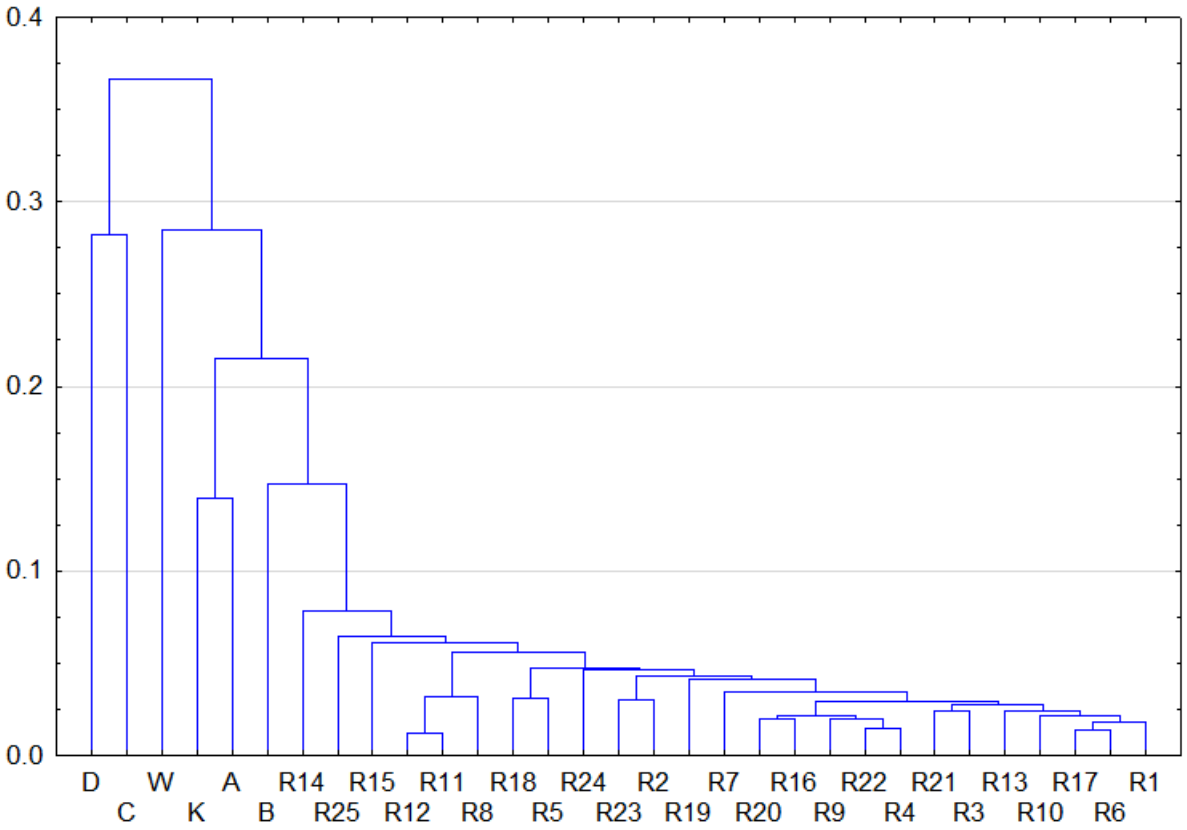

Fig. 20. Dendrogram resulting from the cluster analysis of the intermittency parameter p_0. The vertical scale shows binding distance, whereas the name of gauges is given on horizontal scale (K stands for Kielce gauge, and W stands for Wroclaw).